# Self-Consistent Karplus Parametrization of $^3J$ Couplings Depending on the Polypeptide Side-Chain Torsion $\chi_1$

**Carlos Pérez,[†,§] Frank Löhr,[†] Heinz Rüterjans,[†] and Jürgen M. Schmidt*[,‡]**

*Contribution from the Institut für Biophysikalische Chemie, Johann Wolfgang Goethe-Universität, Biozentrum N230, Marie-Curie-Strasse 9, D-60439 Frankfurt am Main, Germany, and Division of Molecular Structure, National Institute for Medical Research, Mill Hill, London NW7 1AA, United Kingdom*

*Received October 19, 2000. Revised Manuscript Received April 3, 2001*

**Abstract:** Recently proposed self-consistent $^3J$ coupling analysis (Schmidt, J. M.; Blümel, M.; Löhr, F.; Rüterjans, H. *J. Biomol. NMR* **1999**, *14*, 1−12) has been carried out to calibrate Karplus parameters constituting the empirical dependence of $^3J$ coupling constants on the $\chi_1$ dihedral angle in amino acid side chains. The procedure involves simultaneous least-squares optimization of six sets of three Karplus coefficients related to all six $^3J$ coupling types accessible in $^{15}$N,$^{13}$C-labeled proteins. A simple concept of fundamental and incremental component couplings is proposed to account for substituent effects, eventually yielding amino acid topology-specific Karplus parameters. The method is exemplified with recombinant *Desulfovibrio vulgaris* flavodoxin (147 amino acids, 16 kDa) with reference to a total of 749 experimental $^3J_{H\alpha,H\beta}$, $^3J_{N',H\beta}$, $^3J_{C',H\beta}$, $^3J_{H\alpha,C\gamma}$, $^3J_{N',C\gamma}$, and $^3J_{C',C\gamma}$ coupling constants. Unlike other parametrizations, the present method does not make reference to X-ray coordinates, so that the Karplus coefficients obtained are not influenced by differences between solution and crystal states. Cross validation using X-ray torsion angles demonstrates the improvement relative to previous parametrizations. The Karplus coefficients derived are applicable to other proteins, too. Parameter refinement also yields a series of $\chi_1$ torsion angles, providing valuable constraints for protein structure determination, as well as optional parameters of local angular mobility in the contexts of Gaussian random fluctuation or a three-site jump model. The procedure permits automatic stereospecific assignments of $H^\beta$ and $C^\gamma$ chemical shifts. The majority of the flavodoxin side-chain conformations agrees with high-resolution X-ray structures of the protein. Marked deviations between NMR and X-ray datasets are attributed to different rotameric states due to crystal-packing effects and to conformational equilibria between multiple $\chi_1$ rotamers.

## Introduction

Three-bond *J* coupling constants benefit nuclear magnetic resonance (NMR) structure refinement of biological macromolecules. Sets of experimental homo- and heteronuclear $^3J$ coupling constants have been demonstrated to deliver quantitative constraints on backbone torsion angles $\phi$ in proteins[1−3] on the basis of Karplus parameters[4] predetermined with reference to angles from high-resolution X-ray coordinates.[5−7] This assumes that conformations in solution are identical to those in the solid state. Clearly, it would be preferable to use a method that avoided any direct or indirect reference to crystallographic data. In fact, comprehensive sets of $^3J$ coupling constants have recently been converted into accurate protein backbone $\phi$ torsion geometries by applying a self-consistent procedure,[8] without the need for supplementary NOE distance constraints.

The feasibility and success of $\phi$ torsion angle determination so far owe much to two properties unique to the six $\phi$-related *J* coupling types: first, the uniform first-sphere atomic substituent pattern in all amino acid types (except glycine and proline) and, more importantly, the uniform distribution of dihedral angle phases of multiples of $\Delta\phi = 60°$ over the $2\pi$ rotation range due to $sp^2-sp^3$-type carbon centers. When determining amino acid side-chain $\chi_1$ torsions, two hurdles are imminent. First, variation of local topology across different amino acid side chains requires suitable sets of Karplus coefficients be known in order to translate between $^3J$ coupling constants and dihedral angle geometry. Second, leaving aside the intrinsic degeneracy of the Karplus relation, side-chain $\chi_1$-dependent *J* coupling types relate to each other by wider dihedral angle increments of multiples of $\Delta\chi_1 = 120°$, due to $sp^3-sp^3$-type carbon pairs, thus inflicting higher correlation in the structure data than with $\phi$-dependent couplings,[9,10] despite the larger number of up to nine accessible $^3J$ couplings in the polypeptide fragment depicted in Figure 1.

* To whom correspondence should be addressed. Tel.: +44-(20)-8959 3666. Fax: +44-(20)-8906 4477. E-mail: j.schmidt@nimr.mrc.ac.uk.
† Johann Wolfgang Goethe-Universität.
‡ National Institute for Medical Research.
§ Present address: Departimento Quimica Fisica, Universidad de la Habana, Cuba.

(1) Wang, A. C.; Bax, A. *J. Am. Chem. Soc.* **1996**, *118*, 2483−2494.
(2) Hu, J.-S.; Bax, A. *J. Am. Chem. Soc.* **1997**, *119*, 6360−6368.
(3) Blümel, M.; Schmidt, J. M.; Löhr, F.; Rüterjans, H. *Eur. Biophys. J.* **1998**, *27*, 321−334.
(4) Karplus, M. *J. Am. Chem. Soc.* **1963**, *85*, 2870−2871.
(5) Wang, A. C.; Bax, A. *J. Am. Chem. Soc.* **1995**, *117*, 1810−1813.
(6) Hu, J.-S.; Bax, A. *J. Am. Chem. Soc.* **1996**, *118*, 8170−8171.
(7) (a) Pardi, A.; Billeter, M.; Wüthrich, K. *J. Mol. Biol.* **1984**, *180*, 741−751. (b) Ludvigsen, S.; Andersen, K. V.; Poulsen, F. M. *J. Mol. Biol.* **1991**, *217*, 731−736. (c) Vuister, G. W.; Bax, A. *J. Am. Chem. Soc.* **1993**, *115*, 7772−7777.
(8) Schmidt, J. M.; Blümel, M.; Löhr, F.; Rüterjans, H. *J. Biomol. NMR* **1999**, *14*, 1−12.
(9) (a) Hansen, P. E.; Feeney, J.; Roberts, G. C. K. *J. Magn. Reson.* **1975**, *17*, 249−261. (b) Bystrov, V. F.; Gavrilov, Y. D.; Solkan, V. N. *J. Magn. Reson.* **1975**, *19*, 123−129.
(10) Schmidt, J. M. *J. Magn. Reson.* **1997**, 124, 310−322.
(11) IUPAC−IUB Commision on Biochemical Nomenclature. *J. Mol. Biol.* **1970**, *52*, 1−17; *Biochemistry* **1970**, *9*, 3471−3479.

10.1021/ja003724j CCC: $20.00 
Published on Web 06/30/2001

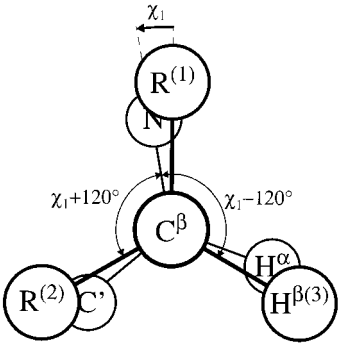


**Figure 1.** Newman projection of a generic amino acid side-chain torsion $\chi_1$ viewed along the $C^{\alpha}-C^{\beta}$ bond axis, set at a nearly eclipsed conformation. Following the IUPAC/IUB recommendations,[11] $\chi_1 = \theta(N-C^{\alpha}-C^{\beta}-R^{(1)}) = -10°$ in the example, as taken from the orientation of the highest-rank substituent, $\gamma$ or $\gamma 1$, with respect to the main-chain atom N′. Disregarding alanine, the majority of the amino acids exhibits the pattern shown with ranked substituents $R^{(1)} = C^{\gamma}$, $R^{(2)} = H^{\beta 2}$, and $H^{\beta 3}$. Atom $C^{\gamma}$ is replaced by $O^{\gamma}$ and $S^{\gamma}$ in serine and cysteine, respectively. For valine residues bearing two carbons in the $C^{\beta}$ position, patches are $R^{(1)} = C^{\gamma 1}$, $R^{(2)} = C^{\gamma 2}$, and $H^{\beta}$. Throughout the present analysis, for the purpose of numerical simplification, torsion angle values in isoleucine and threonine are taken from $\theta(N-C^{\alpha}-C^{\beta}-C^{\gamma 2})$, exempt from the IUPAC/IUB rule according to which substituent ranks are permuted, $R^{(1)} = C^{\gamma 2}$, $R^{(2)} = C^{\gamma 1}$ and $R^{(1)} = C^{\gamma 2}$, $R^{(2)} = O^{\gamma 1}$, respectively. An additive increment of $\Delta\chi_1 = +120°$ is then implied for comparison with other data. Enumerations in parentheses indicate labels needed unless respective positions are uniquely identified.

Translation between coupling constants and the dihedral angle $\theta$ is based on the widely used empirical Karplus relation[4] usually given by $^3J(\theta) = A\cos^2\theta + B\cos\theta + C$. The coefficients critically depend on both the nature of the coupled nuclei and the local chemical environment. They were demonstrated to have a subtle influence on the geometry results,[12] especially when non-negligible dynamic averaging effects on the measured $^3J$ coupling constants impede straightforward data interpretation.[13] Unlike studies on polypeptide-backbone torsions $\phi$, analysis of amino acid side-chain torsions $\chi_1$ can refer to only a few available heteronuclear Karplus curve parametrizations,[14−19] the more so as—to our knowledge—the dihedral angle dependences of several *J*-coupled pairs including $^3J_{N',C\gamma}$ and $^3J_{C',C\gamma}$ have not yet been quantified.

Following early investigations on amino acids at natural $^{13}C$ abundance,[9,20] quantitative *J*-coupling-based studies of polypeptide conformation emerged only later with the advent of convenient isotopic labeling techniques. It is for these reasons that protein side-chain $\chi_1$ torsions obtained to date are merely qualitative or semiquantitative constraints,[21,22] while fully quantitative studies[12,23] have been confined to a few favorable cases, where NOE distance information was also available. This study on $\chi_1$-related $^3J$ couplings in a medium-sized protein pursues both quantitative determination of side-chain $\chi_1$ torsion angles and calibration of all Karplus coefficients associated with all coupling types encountered in the common amino acid side chains, including so far unknown parameters for $^3J_{N',C\gamma}$ and $^3J_{C',C\gamma}$. The method applied extends the novel concept of self-consistent concomitant iteration of Karplus coefficients and torsion angles which proved successful in determining accurate $\phi$ torsion angles and corresponding Karplus parameters without recourse to other than $^3J$ coupling information.[8]

## Method

To facilitate both numerical parameter optimization and interpretation of the results, the commonly used cosine power representation of the empirical Karplus relation shall be cast into a series of (real) Fourier coefficients truncated after the third term, as originally proposed,[4]

$$^3J(\theta) = C_0 + C_1\cos\theta + C_2\cos 2\theta \qquad (1)$$

so that the identities $A = 2C_2$, $B = C_1$, and $C = C_0 - C_2$ restore the coefficients of the power series. $C_0$ is the mean value of *J* invariantly obtained upon complete revolution of $\theta$ over the $2\pi$ interval. Primary and secondary maxima of the Karplus curve, i.e., trans and cis orientations of the dihedral angle $\theta$, respectively, differ by $2C_1$ (normally negative). The largest deflection in *J* from the mean amounts to $(C_2 - C_1)$. Of practical use are *J* values associated with trans and gauche orientations as given by $(C_0 - C_1 + C_2)$ and $(C_0 + C_1/2 - C_2/2)$, respectively. Such Fourier-type parametrization has the unique property of gathering the *average coupling magnitude* in the angle-independent coefficient $C_0$, whereas $C_1$ and $C_2$ terms average identically zero on full rotation.

Conventional parametrization of the torsion angle dependence of $^3J$ couplings requires that experimental values of *J* be referred to dihedral angle values $\theta$ derived from high-resolution X-ray coordinates of model compounds. Both coupling constant and dihedral angle are fixed values, confining parametrization on the basis of eq 1 to adjusting coefficients $C_m$, $m = 0, 1, 2$, as the only variables to accomplish the best possible match between prediction and experiment. In a notional plot of *J* vs $\theta$, regression discrepancies between back-calculated *J* values and experimental ones, i.e., residuals $\epsilon_J$, would vary along the *y*-direction only. When reference conformations in solution and in the solid state do not agree, resulting Karplus curves are notoriously prone to distortion. Too shallow a curvature is caused by the neglect of angular dynamics effects[10,13,24] when present in the dissolved sample but not possibly in the solid state. Coefficients $C_1$ and $C_2$ tend to exaggerate curve amplitudes if sampling of the dihedral angle interval is sparse or nonuniform in the experimental set.[1] If fixed dihedral angle values were abandoned and back-calculated spots $J(\theta)$ were permitted to move freely along perpendicular directions in the graph, less biased Karplus curves would be achieved. The fit error then amounts to some composite residual as a result of both residuals $\epsilon_\theta$ and $\epsilon_J$ sensing dihedral angle variation (parallel to the *x* axis) and adjustment of Karplus coefficients (along *y* as before), respectively. In fact, reference dihedral angles become obsolete when fitting sets of Karplus coefficients to multiple phase-shifted $^3J$ coupling types simultaneously rather than one

(12) Karimi-Nejad, Y.; Schmidt, J. M.; Rüterjans, H.; Schwalbe, H.; Griesinger, C. *Biochemistry* **1994**, *33*, 5481−5492.
(13) (a) Jardetzky, O. *Biochim. Biophys. Acta* **1980**, 621, 227−232. (b) Hoch, J. C.; Dobson, C. M.; Karplus, M. *Biochemistry* **1985**, *24*, 3831−3841.
(14) Bystrov, V. F. *Prog. NMR Spectrosc.* **1976**, *10*, 41−81.
(15) DeMarco, A.; Llinás, M.; Wüthrich, K. *Biopolymers* **1978**, *17*, 617−636.
(16) Fischman, A. J.; Live, D. H.; Wyssbrod, H. R.; Agosta, W. C.; Cowburn, D. *J. Am. Chem. Soc.* **1980**, *102*, 2533−2539.
(17) Wasylishen, R.; Schaefer, T. *Can. J. Chem.* **1972**, *50*, 2710−2712.
(18) Kopple, K. D.; Wiley, G. R.; Tauke, R. *Biopolymers* **1973**, *12*, 627−636.
(19) DeMarco, A.; Llinás, M.; Wüthrich, K. *Biopolymers* **1978**, *17*, 2727−2742.
(20) Feeney, J.; Hansen, P. E.; Roberts, G. C. K. *J. Chem. Soc., Chem. Commun.* **1974**, 465−466.
(21) (a) Nagayama, K.; Wüthrich, K. *Eur. J. Biochem.* **1981**, *115*, 653−657. (b) Boyd, J.; Redfield, C. *J. Magn. Reson.* **1986**, *68*, 67−84. (c) Hyberts, S. G.; Märki, W.; Wagner, G. *Eur. J. Biochem.* **1987**, *164*, 625−635. (d) Smith, L. J.; Sutcliffe, M. J.; Redfield, C.; Dobson, C. M. *Biochemistry* **1991**, *30*, 986−996. (e) Xu, R. X.; Olejniczak, E. T.; Fesik, S. W. *FEBS* **1992**, *305*, 137−143.
(22) Hennig, M.; Bermel, W.; Spencer, A.; Dobson, C. M.; Smith, L. J.; Schwalbe, H. *J. Mol. Biol.* **1999**, 288, 705−723.
(23) (a) Dzakula, Z.; Westler, W. M.; Edison, A.; Markley, J. *J. Am. Chem. Soc.* **1992**, *114*, 6195−6199. (b) Dzakula, Z.; Edison, A.; Westler, W. M.; Markley, J. *J. Am. Chem. Soc.* **1992**, *114*, 6200−6207. (c) Polshakov, V. I.; Frenkiel, T. A.; Birdsall, B.; Soteriou, A.; Feeney, J. *J. Magn. Reson. B* **1995**, *108*, 31−43.
(24) Brüschweiler, R.; Case, D. A. *J. Am. Chem. Soc.* **1994**, *116*, 11199−11200.

at a time. Consequently, calculated $J$ values become *recursively* dependent on Karplus coefficients and dihedral angles, both of which, once primed with suitable values, are then found iteratively in a numerical procedure dubbed self-consistent $J$ coupling analysis.[8]

The method outlined takes advantage of redundant structure information inherent in large sets of related types of $^3J$ coupling constants, referred to as the sole experimental foundation. The interplay between variable Karplus coefficients and dihedral angles linked by (constant) experimental $J$ values is best illustrated by a spreadsheet of functions $J(C_m,\theta)$, i.e., a matrix of cells, each one of them displaying a $J$ value predicted according to eq 1 as a result of parameters $\theta(J,C_m)$ and $C_m(J,\theta)$ acting on row and column elements, respectively.[25] Simultaneous optimization of all the control variables, $\theta$ and $C_m$, is then driven by fit deviations, from all the experimental $^3J$ coupling constants, continuously redistributed to minimize the summed square residual $\epsilon_J^2$.

Methods were applied to the 147-amino-acid electron-transfer protein *Desulfovibrio vulgaris* flavodoxin (16.3 kDa), the biochemical properties of which have been extensively reviewed.[26] Crystallographic studies of the Ala$^2$Pro mutant delivered 0.19-nm resolution models of *D. vulgaris* flavodoxin containing a noncovalently bound flavine mononucleotide (FMN) prosthetic group in the oxidized state at ambient and low temperatures, referred to as protein database entries 2FX2 and 3FX2, respectively.[27] An additional coordinate set of the wild-type sequence, used for comparison with the NMR results, has been refined by Walsh at 0.17 nm resolution.[28] The refinement state of the solution structure hitherto comprises interproton distances obtained from homonuclear and $^1$H,$^{15}$N-heteronuclear NMR spectra[29,30] as well as accurate backbone torsion angle constraints[3,8] on the basis of comprehensive sets of $\phi$-related $^3J$ coupling constants.

## Results

The polypeptide side-chain fragment of two tetrahedral centers X−C$^\alpha$−C$^\beta$−Y, with X being either N′ or C′ or H$^\alpha$ and Y substituting for one out of C$^{\gamma(1)}$, C$^{\gamma 2}$, H$^{\beta(2)}$, or H$^{\beta 3}$ (Figure 1), gives rise to 12 different coupled types $^3J_{X,Y}$ related to the dihedral angle $\chi_1$. For the protein *D. vulgaris* flavodoxin,[26] nearly complete sets of all these homo- and heteronuclear $^3J$ coupling constants, 180 $^3J_{H\alpha,H\beta}$, 168 $^3J_{N',H\beta}$, 153 $^3J_{C',H\beta}$, 84 $^3J_{H\alpha,C\gamma}$, 83 $^3J_{N',C\gamma}$, and 82 $^3J_{C',C\gamma}$, have been collected from a series of 3D heteronuclear NMR experiments carried out using a $^{15}$N,$^{13}$C-doubly enriched sample. For 17 out of 112 residues bearing rotatable side chains, the maximum nine quantitative $^3J$ coupling constants were available. Another 20, 26, 13, 14, and 5 residues contributed between eight and four coupling constants, respectively. No more than six coupling constants define the side-chain conformations of the 19 cysteine, serine, and threonine residues present in flavodoxin, so 951 $\chi_1$-related $^3J$ coupling constants are expected at most. Excluded from the analysis were 15 residues exhibiting degenerate H$^\beta$ chemical shifts because the three remaining C$^\gamma$-related coupling constants alone do not allow dihedral angles to be determined reliably. To improve estimates for the angle-independent Karplus coefficients $C_0$, rotationally averaged H$^\beta$-related $J$ coupling constants from all 17 alanine residues were included by duplicating each set as if coupling constants had been measured twice. Although of no relevance to molecular modeling, alanine torsions fitted then typically adopted $\chi_1 \approx \pm 120°$, a condition for which contributions from the angle-dependent terms $C_1 \cos\theta$ and $C_2 \cos 2\theta$ nearly cancel. Group averages of the alanine coupling constants, $\langle {}^3J_{H\alpha,H\beta}\rangle = 5.88 \pm 0.20$ Hz, $\langle {}^3J_{N',H\beta}\rangle = 2.61 \pm 0.24$ Hz, and $\langle {}^3J_{C',H\beta}\rangle = 3.96 \pm 0.15$ Hz, hinted at an experimental standard error of $\sigma_J = 0.50$ Hz for the single $J$ coupling measurement (square root of twice the summed group variances).

**Conventional Calibration of Karplus Coefficients against Static X-ray Coordinates.** At first, Karplus parameters constituting the dihedral angle dependence of $\chi_1$-related couplings were conventionally obtained from the $J$ coupling data, referencing (fixed) torsion values calculated from recent X-ray coordinates of wild-type *D. vulgaris* flavodoxin.[28] A linear least-squares method was applied separately to each coupling type. Accordingly, coefficients for the dihedral angle dependence of $^3J_{H\alpha,H\beta}$ in the commonly used cosine power representation were $(A, B, C) = (3.47, -1.61, 4.33$ Hz), with overall violations in the $J$ coupling constants of $\mathrm{RMSD}_J = 1.18$ Hz and a normalized square residual $\epsilon_J^2 = 1898.1$. Results were marginally better ($\mathrm{RMSD}_J = 0.90$ Hz) for $^3J_{H\alpha,C\gamma}$ coefficients (2.70, −0.79, 1.77). Parametrization of C′-related couplings $^3J_{C',H\beta}$ and $^3J_{C',C\gamma}$ yielded coefficients (2.81, −0.97, 1.60) and (1.25, −0.74, 1.36), with average discrepancies of 0.77 and 0.75 Hz, respectively. Owing to their small absolute magnitudes, N′-related couplings $^3J_{N',H\beta}$ and $^3J_{N',C\gamma}$ produced the smallest discrepancies between NMR and X-ray datasets, namely 0.57 and 0.34 Hz with coefficients (2.21, −0.33, 1.05) and (0.86, −0.41, 0.59), respectively.[31] The disappointing overall fit error of 0.8 Hz per coupling constant exceeds expectations and experimental precision alike. Stereospecific H$^\beta$ and C$^\gamma$ resonance assignments (SSA) have been permuted at best, separately for each coupling type though. Had they been permuted in a concerted fashion, results would have deteriorated.

**Self-Consistent $J$ Coupling Analysis of *D. vulgaris* Flavodoxin Side-Chain Conformations.** More accurate determination of Karplus parameters was accomplished by the recently proposed self-consistent $J$ coupling evaluation procedure[8] extended to include stereospecific assignment swapping. The concept critically taps into the redundancy intrinsic in the $J$ coupling dataset that arises from multiple $J$ determinations for each dihedral angle.

The symmetry introduced by the mirror-image dihedral angle dependence $J(\theta)$ with respect to $\theta = 0°$ demands a minimum

(25) Details of such a matrix layout and the numerical least-squares protocols have been given in ref 8. In present $\chi_1$ determinations, columns relating to the six $J$ coupling types involved are duplicate such as to enable permuting $^3J$ values in the reference set for stereospecific assignments of H$^\beta$ or C$^\gamma$ resonance pairs, if applicable. $J$ coupling data are therefore arranged in a matrix the size of $K \times 12$ with experimental coupling constants, $J_{k,l}^{\mathrm{expt}}$, of residue $k$ (out of $K$ total) and coupling type $l$. Dynamic Gaussian averaging effects on the model $^3J$ coupling constants were imposed on Fourier components in eq 1, replacing them with convolution terms, $\langle \cos m\theta\rangle = \mathrm{e}^{-m^2\sigma_\theta^2/2} \cos m\theta$, where $m = 0, 1, 2$, benefiting from the readily vectorizable identity, $\langle \cos m\theta\rangle = Re\{\mathrm{e}^{im\chi_1 - m^2\sigma_\theta^2/2}\, \mathrm{e}^{im\Delta\chi_1}\}$, with $\theta = \chi_1 + \Delta\chi_1$. Karplus coefficients and Gaussian width parameters were both fitted in the logarithm as to avoid the need to constrain variables to positive numbers. Likewise, probabilities $p_1$ and $p_2$ of the three-site jump model were transformed using the logistic sigmoid, $p_i = (1 + \mathrm{e}^{-p_i'})^{-1}$, as to maintain $p_i$ in the [0,1] interval on unrestricted variation of $p_i'$.

(26) (a) Mayhew, S. G.; Ludwig, M. L. Flavodoxin and Electron-Transferring Flavoproteins. In *The Enzymes*, 3rd ed.; Boyer, P. D., Ed.; Academic Press: New York, 1975; Vol. 12, pp 57−118. (b) Dubourdieu, M.; Fox, J. L. *J. Biol. Chem.* **1977**, *252*, 1453−1459. (c) Ghisla, S.; Massey, V. *Eur. J. Biochem.* **1989**, *181*, 1−17. (d) Mayhew, S. G.; Tollin, G. In *Chemistry and Biochemistry of Flavoenzymes*, 3rd ed.; Müller, F., Ed.; CRC Press: Boca Raton, FL, 1992; Vol. 3, pp 389−426.

(27) Watt, W.; Tulinsky, A.; Swenson, R. P.; Watenpaugh, K. D. *J. Mol. Biol.* **1991**, *218*, 195−208.

(28) (a) Walsh, M. A. Ph.D. Thesis, National University of Ireland, 1994. (b) Walsh, M. A.; McCarthy, A.; O'Farrell, P. A.; McArdle, P.; Cunningham, P. D.; Mayhew, S. G.; Higgins, T. M. *Eur. J. Biochem.* **1998**, *258*, 362−371.

(29) (a) Knauf, M. A.; Löhr, F.; Curley, G. P.; O'Farrell, P.; Mayhew, S. G.; Müller, F.; Rüterjans, H. *Eur. J. Biochem.* **1993**, *213*, 167−184. (b) Knauf, M. A.; Löhr, F.; Blümel, M.; Mayhew, S. G.; Rüterjans, H. *Eur. J. Biochem.* **1996**, *238*, 423−434.

(30) Stockman, B. J.; Richardson, T. E.; Swenson, R. P. *Biochemistry* **1994**, *33*, 15298−15308.

(31) For the sake of numerical unification, negative and positive values are adopted here for odd and even indexed coefficients, respectively, knowing that the negative gyromagnetic ratio of nitrogen inverts sign.

**Table 1.** Statistics on Self-Consistent Models for *J* Couplings and Side-Chain Torsion Angles $\chi_1$ in *Desulfovibrio vulgaris* Flavodoxin

| | | NMR[a] | | | | | | X-ray[b] | | |
|---|---|---|---|---|---|---|---|---|---|---|
| | | $J_4M_0S_0$ | $J_4M_0S_1$ | $J_4M_1S_0$ | $J_4M_1S_1$ | $J_4M_2S_0$ | $J_4M_2S_1$ | Walsh | 2FX2 | 3FX2 |
| $RMSD_J$ (Hz) | | 0.54 | 0.48 | 0.48 | **0.40** | 0.50 | 0.42 | 0.82 | 0.81 | 0.87 |
| $RMSD_\theta$ (deg) | | 50.8 | 51.9 | 49.0 | **41.8** | na | na | 0 | 0 | 0 |
| number of adjustables ($p$) | | 130 | 137 | 242 | **249** | 242 | 249 | 18 | 18 | 18 |
| degrees of freedom ($n - p$) | | 633 | 626 | 521 | **514** | 521 | 514 | 681 | 676 | 676 |
| normalized fit error $\epsilon_J^2$ | | 891.8 | 705.6 | 699.1 | **500.2** | 751.5 | 546.4 | 1898.1 | 1799.4 | 2125.2 |
| abs. significance[c] $Q$ (%) (diagonal) | | | | | | | | | | |
| rel. significance[d] $P$ (%) (off-diagonal) | $J_4M_0S_0$ | 0 | | | | | | | | |
| | $J_4M_0S_1$ | 0 | 1 | | | | | | | |
| | $J_4M_1S_0$ | 0 | 91 | 0 | | | | | | |
| | $J_4M_1S_1$ | 0 | 0 | 0 | **66** | | | | | |
| | $J_4M_2S_0$ | 4 | 45 | 41 | 0 | 0 | | | | |
| | $J_4M_2S_1$ | 0 | 0 | 1 | 32 | 0 | 16 | | | |
| | Walsh | 0 | 0 | 0 | 0 | 0 | 0 | 0 | | |
| | 2FX2 | 0 | 0 | 0 | 0 | 0 | 0 | 49 | 0 | |
| | 3FX2 | 0 | 0 | 0 | 0 | 0 | 0 | 10 | 2 | 0 |

[a] Self-consistent *J* coupling calibrations using a minimum of four coupling constants per residue ($J_4$), excluding ($S_0$, $6 \times 3$ fundamental Karplus coefficients) or including ($S_1$, 7 additional incremental coefficients, see text) substituent effects, with no angular motion ($M_0$), Gaussian-random fluctuation ($M_1$), or according to a three-site jump model ($M_2$). [b] Conventional *J* coupling calibrations using reference torsion angles from X-ray coordinates. "Walsh" denotes the structure of the wild-type *D. vulgaris* flavodoxin−FMN complex (oxidized) resolved at 0.17 nm by Dr. Martin Walsh (EMBL-Hamburg). Coordinate sets 2FX2 and 3FX2 (PDB) of the Pro2Ala mutant protein from data taken at ambient temperature and 123 K were both resolved at 0.19 nm and refined with *R* factors of 0.17 and 0.20, respectively, according to ref 27. [c] Absolute significances in the framework of $\chi^2$ statistics (diagonal entries of the comparison matrix) are based on a test of the incomplete $\Gamma$ probability distribution function (see ref 10 and literature cited therein). The percentage, $Q = 1 - P$, derives from the probability, $P = \Gamma(\chi^2/2, \nu/2)$, of rejecting the hypothesis that the fitted parameter set is a chance incidence. As a rule of thumb, $P \approx 0.5$ if the *normalized* $\chi^2$ error (denoted $\epsilon_J^2$ in the present work to avoid confusion with torsion angle notations) approaches the number of degrees of freedom, $\nu$, in the model. [d] Relative significances in the framework of *F*-statistics (off-diagonal entries in the comparison matrix) are based on the *F*-test involving pairwise $\epsilon_J^2$ ratios and associated numbers of degrees of freedom (see ref 32 and literature cited therein). In a statistical sense, any two models differ significantly if the probability, *P*, is small, such as to yield a measure of increased correlation for higher probabilities. Note that the absence of Pro2 reduces the number of coupling constraints in sets 2FX2 and 3FX2 as compared to the set of wild-type sequence.

set of experimental data per dihedral angle to resolve the ambiguity intrinsic in the Karplus relation.[3,10] Optimizations were tried out for a range of thresholds from three to eight coupling constants per residue, only to result in no particular improvement with higher over smaller numbers as fewer and fewer side chains, and therefore fewer experimental data, are included. Torsion angles of residues contributing numerous couplings converged at similar values irrespective of the actual threshold applied. Side chains contributing fewer than four experimental constraints tended to lock into arbitrary conformations, contributing negligible error with no adverse effects on the Karplus coefficients though. Only by chance would torsion angle values delivered for these residues be correct, as ambiguous, nearly eclipsed $\chi_1 = 0°$ or $\pm 120°$ conformations were typically obtained. Eventually, a minimum of four coupling constraints per residue (model identifier $J_4$) was found most suitable.

Basic self-consistent analysis of the $\chi_1$-related *J* couplings in *D. vulgaris* flavodoxin required $6 \times 3$ Karplus coefficients and 95 relevant non-alanine and 17 auxiliary alanine torsion angles to be adjusted simultaneously, so that the number of fit parameters was $p = 130$, referencing $n = 763$ experimental *J* values (including 50 duplicate alanine couplings). A global $RMSD_J$ of 0.54 Hz between back-calculated and experimental coupling constants was achieved (Table 1), significantly smaller than that obtained with the conventional calibration method used before. Apart from experimental random error, remaining discrepancies between back-calculated and experimental $^3J$ coupling constants originate from a range of factors neglected in the model including angular mobility, substituent patterns, hybridization or other electronic effects, and distortions of the central tetrahedral $C^\alpha$ and $C^\beta$ sites. Perfect tetrahedral geometry at $C^\alpha$ carbons is taken for granted.[2,8] To assess possible static distortions of $C^\beta$ sites, mean dihedral angle differences between the two heavy-atom branches of valine, isoleucine, and threonine were computed from X-ray coordinate sets available for *D. vulgaris* flavodoxin, 2FX2,[27] 3FX2,[27] and wild-type,[28] yielding $121.6 \pm 6.0°$, $125.1 \pm 8.2°$, and $120.2 \pm 4.5°$, respectively. Such small deviations from the anticipated mean of 120° place least priority on $C^\beta$ tetrahedral distortion, and we assume perfect bonding geometry hence.

**Probability Distribution Functions To Account for Angular Mobility.** Advanced modeling accounts for $\chi_1$ angular mobility by supplying each torsion angle with a Gaussian probability distribution function (model identifier $M_1$).[10,12,13] The additional width parameters $\sigma_\theta$ (in radians) raised the number of fit variables to $p = 242$. Alternatively, a three-site jump between staggered rotamers with $\chi_1$ fixed at −60°, 180°, and +60° was modeled (identifier $M_2$) with two adjustable probabilities $p_1$, $p_2$, and the derived probability $p_3 = (1 - p_1 - p_2)$, respectively. The additional mobility parameters improved the fit between simulated and experimental coupling constants at $RMSD_J = 0.48$ Hz (Table 1). However, fit residuals were found to correlate strongly with amino acid type in both rigid and Gaussian libration models (Figure 2A,B). For example, every single coupling measurement in serine, cysteine, and threonine residues was, on average, smaller by 0.4 Hz than predicted from the fitted Karplus curves. Half of the $^3J_{H\alpha,H\beta}$ couplings in serines contributed approximately −1 Hz each to the deviation, and a few $^3J_{C',H\beta}$ couplings were off by almost −2 Hz. The significant negative bias on the order of the experimental precision mainly reflects the electron-withdrawing effect of oxygen and sulfur substituents attached to the intervening $C^\beta$ atom. In contrast, experimental coupling constants in aspartate and asparagine residues showed a similar yet positive bias, apparently because of combined electronic effects from terminal nitrogen and/or oxygen substituents and the $sp^2$-hybridized $C^\gamma$ atom. Typically, $^3J_{C',C\gamma}$ couplings in Asx residues were larger than the back-calculated values by as much as 1−2 Hz. Thus, it became apparent that substituent effects are critical to $\chi_1$ dihedral angle analysis, in addition to mobility effects (Figure 2C,D).

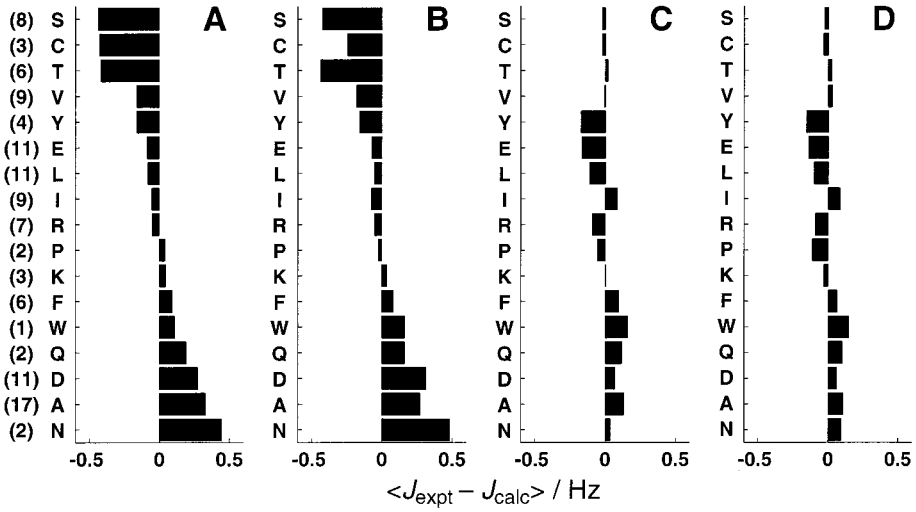


**Figure 2.** Residue-specific bias in experimental *J* coupling constants as compared with values back-calculated in self-consistent $\chi_1$ torsion angle optimizations for *D. vulgaris* flavodoxin. Signed *J* coupling constraint violations are averaged over all contributing entries, separately for each amino acid type, as indicated by one-letter codes. Amino acid frequencies in the fit are given in parentheses, where glycine, histidine, and methionine are absent in the current *J* coupling dataset. The underlying models involve (A) rigid torsions and 6 × 3 basic Karplus coefficients ($J_4M_0S_0$); (B) as before, including angular Gaussian random fluctuation ($J_4M_1S_0$); (C) rigid torsions, 6 × 3 fundamental and 7 incremental substituent-specific Karplus coefficients $\Delta C_0$ ($J_4M_0S_1$); and (D) as before, including angular mobility ($J_4M_1S_1$).

**Fundamental and Incremental Karplus Coefficients To Account for Amino Acid Topology.** The six fitted sets of basic Karplus coefficients are associated with various pair combinations of directly interacting atom types N, C, and H only. Except for the traditional distinction between H,C-heteronuclear coupling constants $^3J_{C',H\beta}$ and $^3J_{H\alpha,C\gamma}$, no effort was made so far to account for variation of substituents with amino acid topology. The empirical measure of substituent effects in a given coupling path is the coupling increment $\Delta J^R_{X,Y} = J^R_{X,Y} - J^H_{X,Y}$ inferred from the experimental coupling constants $J^R_{X,Y}$ and $J^H_{X,Y}$ taken from substituted and unsubstituted compounds, respectively,[33] denoting the change in the coupling $^3J_{X,Y}$ on substituting a heavy atom or a group of atoms for a notional hydrogen atom. Incremental Karplus parameters, also known as component couplings, are likely to depend on both the substituent's type and its relative position.[34] In an attempt to reduce the fit error further still, the amino-acid-type-independent set of Karplus coefficients $C_m$ obtained has been supplemented by respective increments $\Delta C_m$. In the present work, two categories comprising "inner" and "outer" substituents were established to represent modifications made to central ($C^\alpha$ and $C^\beta$) and terminal sites (X and Y), respectively.

Since incremental Karplus coefficients established were introduced merely to reflect topology and were supposed not to depend on the type of the basic X−Y combination, any one substituent-specific parameter $\Delta C$ would, in a uniform manner, apply to all six coupling types involved in $\chi_1$ analysis. However, average coupling magnitudes do vary with *J* coupling type such as to necessitate proper scaling of the incremental effect. For example, $^3J_{H\alpha,C\gamma}$ coupling constants usually exceed values of $^3J_{N',C\gamma}$ on an absolute measure, so that an "outer" substituent, for instance oxygen attached to $C^\gamma$, is expected to have larger effects on the former coupling than on the latter. Similarly, "inner" $C^\beta$-bound substituents will affect large $^3J_{H\alpha,H\beta}$ couplings more than small $^3J_{N',H\beta}$ couplings. Mean coupling magnitudes, as obtained on complete torsion revolution and expressed by the fundamental coefficients $C_0$, seemingly correlate with the product gyromagnetic ratio of the actively coupled nuclei, leading to coupling-type-dependent weights used to normalize the incremental effect, $\Delta C_0$, a substituent may have on the various X−Y pair combinations, as given by

$$w = (\gamma_X \gamma_Y)^{1/2} \gamma_H^{-1} \quad (2)$$

The numerical implementation further involves amino-acid-dependent increment counts, *N*, related to the number and covalent bond order of respective substituents (see Supporting Information), the functional form of the *J* coupling model then being

$$^3J(\theta) = C_0 + w\sum(N\Delta C_0) + C_1 \cos\theta + C_2 \cos 2\theta \quad (3)$$

In the present work, the combination of 18 fundamental Karplus coefficients and 7 angle-independent increments $\Delta C_0$, as compiled in Table 2 and Table 3, sufficiently accounted for topology effects from all common amino acid types. Trial fits including angle-dependent $\Delta C_1$ and $\Delta C_2$ increments, too (seven each), showed symptoms characteristic of overparametrization. Strong anti-correlation was present among both additional parameter types, in particular for increments associated with "inner H → S" and "outer H → N" replacements due to less abundant cysteine and asparagine residues, respectively. In line with previous experience,[35] correlation of the remaining *J* coupling discrepancy with dihedral angle was virtually absent, due perhaps to the limited number of residues in the fit. This provided justification for confining corrective coefficients to $C_0$, implying that substituent-related amendments would affect the angle-invariant mean coupling magnitude only.

Residue-specific Karplus coefficients improved the fit error by about 25% with respect to the basic calculation disregarding topology ($J_4M_0S_1$ vs $J_4M_0S_0$). Extreme *J* coupling violations originating from serine, threonine, asparagine, and aspartate side chains were especially removed (Figure 2C). Results improved further when mobility was included (Figure 2D), for which

(32) Schmidt, J. M. *J. Magn. Reson.* **1997**, *124*, 298−309.
(33) Krivdin, L. B.; Della, E. W. *Prog. NMR Spectrosc.* **1991**, *23*, 301−610.
(34) (a) Hansen, P. E. *Prog. NMR Spectrosc.* **1981**, *14*, 175−296. (b) Hansen, P. E. *Org. Magn. Reson.* **1978**, *5*, 215−233.
(35) Severson, M. L.; Maciel, G. E. *J. Magn. Reson.* **1984**, *57*, 248−268.

**Table 2.** Amino-Acid-Specific $\chi_1$-Related Karplus Coefficients As Inferred from Self-Consistent *J* Coupling Analysis of Flavodoxin Data

| | | Fourier coefficients[c] | | | cos power coefficients[d] | | | staggered states | |
|---|---|---|---|---|---|---|---|---|---|
| *J* type[a] | $\chi_1$ substituent pattern[b] | $C_0$ | $C_1$ | $C_2$ | $A$ | $B$ | $C$ | $J_{trans}$ | $J_{gauche}$ |
| $^3J_{H\alpha,H\beta}$ | *fundamental* | *7.24* | | | | | *3.62* | *12.2* | *4.8* |
| | Ala | 6.63 | | | | | 3.01 | 11.6 | 4.1 |
| | Arg, Asx, Glx, His, Leu, Lys, Met, Phe, Pro, Trp, Tyr | 6.01 | | | | | 2.40 | 11.0 | 3.5 |
| | **consensus** | **5.83** | **−1.37** | **3.61** | **7.23** | **−1.37** | **2.22** | **10.8** | **3.3** |
| | Ile, Val | 5.40 | | | | | 1.79 | 10.4 | 2.9 |
| | Cys | 5.32 | | | | | 1.71 | 10.3 | 2.8 |
| | Ser | 5.03 | | | | | 1.42 | 10.0 | 2.5 |
| | Thr | 4.42 | | | | | 0.81 | 9.4 | 1.9 |
| $^3J_{N',H\beta}$ | *fundamental* | *2.72* | | | | | *1.57* | *4.6* | *1.8* |
| | Ala | 2.47 | | | | | 1.32 | 4.4 | 1.5 |
| | Arg, Asx, Glx, His, Leu, Lys, Met, Phe, Trp, Tyr | 2.28 | | | | | 1.13 | 4.2 | 1.3 |
| | Pro | 2.23 | | | | | 1.08 | 4.1 | 1.3 |
| | **consensus** | **2.22** | **−0.75** | **1.15** | **2.30** | **−0.75** | **1.07** | **4.1** | **1.3** |
| | Ile, Val | 2.08 | | | | | 0.93 | 4.0 | 1.1 |
| | Cys | 2.06 | | | | | 0.91 | 4.0 | 1.1 |
| | Ser | 1.97 | | | | | 0.81 | 3.9 | 1.0 |
| | Thr | 1.77 | | | | | 0.62 | 3.7 | 0.8 |
| $^3J_{C',H\beta}$ | Ala | 3.72 | | | | | 1.71 | 7.3 | 1.7 |
| | Arg, Asx, Glx, His, Leu, Lys, Met, Phe, Pro, Trp, Tyr | 3.41 | | | | | 1.41 | 7.0 | 1.4 |
| | **consensus** | **3.32** | **−1.58** | **2.01** | **4.02** | **−1.58** | **1.32** | **6.9** | **1.3** |
| | Ile, Val | 3.11 | | | | | 1.10 | 6.7 | 1.1 |
| | Cys | 3.07 | | | | | 1.06 | 6.7 | 1.1 |
| | Ser | 2.92 | | | | | 0.91 | 6.5 | 0.9 |
| | Thr | 2.62 | | | | | 0.61 | 6.2 | 0.6 |
| | *fundamental* | *2.21* | | | | | *0.20* | *5.8* | *0.4* |
| $^3J_{H\alpha,C\gamma}$ | Asn | 5.09 | | | | | 2.42 | 8.7 | 3.3 |
| | Asp | 4.48 | | | | | 1.81 | 8.1 | 2.7 |
| | His | 4.32 | | | | | 1.65 | 8.0 | 2.5 |
| | *fundamental* | *3.88* | | | | | *1.21* | *7.5* | *2.1* |
| | Met | 3.57 | | | | | 0.90 | 7.2 | 1.8 |
| | Arg, Glx, Lys, Pro | 3.49 | | | | | 0.82 | 7.1 | 1.7 |
| | **consensus** | **3.46** | **−0.96** | **2.67** | **5.34** | **−0.96** | **0.79** | **7.1** | **1.6** |
| | Leu | 3.41 | | | | | 0.74 | 7.0 | 1.6 |
| | Phe, Trp, Tyr | 3.33 | | | | | 0.67 | 7.0 | 1.5 |
| | Val | 3.26 | | | | | 0.60 | 6.9 | 1.5 |
| | Ile | 3.18 | | | | | 0.52 | 6.8 | 1.4 |
| | Thr | 2.77 | | | | | 0.10 | 6.4 | 1.0 |
| $^3J_{N',C\gamma}$ | Asn | 1.54 | | | | | 0.89 | 2.7 | 1.0 |
| | Asp | 1.35 | | | | | 0.70 | 2.5 | 0.8 |
| | His | 1.30 | | | | | 0.65 | 2.4 | 0.7 |
| | *fundamental* | *1.18* | | | | | *0.53* | *2.3* | *0.6* |
| | Met | 1.06 | | | | | 0.41 | 2.2 | 0.5 |
| | Arg, Glx, Lys | 1.03 | | | | | 0.39 | 2.2 | 0.5 |
| | **consensus** | **1.02** | **−0.49** | **0.65** | **1.29** | **−0.49** | **0.37** | **2.2** | **0.5** |
| | Leu, Pro | 1.01 | | | | | 0.36 | 2.2 | 0.4 |
| | Phe, Trp, Tyr | 0.98 | | | | | 0.34 | 2.1 | 0.4 |
| | Val | 0.96 | | | | | 0.31 | 2.1 | 0.4 |
| | Ile | 0.93 | | | | | 0.29 | 2.1 | 0.4 |
| | Thr | 0.80 | | | | | 0.16 | 1.9 | 0.2 |
| $^3J_{C',C\gamma}$ | Asn | 2.52 | | | | | 1.37 | 4.5 | 1.5 |
| | Asp | 2.22 | | | | | 1.06 | 4.2 | 1.2 |
| | His | 2.14 | | | | | 0.98 | 4.2 | 1.1 |
| | Met | 1.76 | | | | | 0.61 | 3.8 | 0.8 |
| | Arg, Glx, Lys, Pro | 1.72 | | | | | 0.57 | 3.8 | 0.7 |
| | **consensus** | **1.70** | **−0.87** | **1.15** | **2.31** | **−0.87** | **0.55** | **3.7** | **0.7** |
| | Leu | 1.68 | | | | | 0.53 | 3.7 | 0.7 |
| | Phe, Trp, Tyr | 1.64 | | | | | 0.49 | 3.7 | 0.6 |
| | Val | 1.61 | | | | | 0.45 | 3.6 | 0.6 |
| | Ile | 1.57 | | | | | 0.41 | 3.6 | 0.6 |
| | Thr | 1.36 | | | | | 0.21 | 3.4 | 0.4 |
| | *fundamental* | *1.00* | | | | | *−0.15* | *3.0* | *0.0* |

[a] See Figure 1 legend for the definition of $\gamma 1$ and $\gamma 2$ positions in valine vs isoleucine/threonine. [b] Amino-acid-independent fundamental Karplus parameters are valid for fully hydrogenated model fragments. Augmented by appropriate increments obtained in the same analysis (Table 3) using weights depending on amino acid topology (see Supporting Information), they give rise to amino-acid-specific Karplus parameters. Consensus coefficients are averages over all 95 residues in the fit, weighted by their fractional occurrence: Ala (17), Arg (7), Asn (2), Asp (11), Cys (3), Gln(2), Glu (11), His (0), Ile (9), Leu (11), Lys (3), Met (0), Phe (6), Pro (2), Ser (8), Thr (6), Trp (1), Tyr (4), Val (9). [c] Coefficients (in Hz) for use with eq 1, $^3J(\theta) = C_0 + C_1 \cos\theta + C_2 \cos 2\theta$, where $\theta = \chi_1 + \Delta\chi_1$, according to Figure 1, and coefficients $C_0$ already comprise incremental effects according to eq 3. Results from calculations including substituent effects and Gaussian random fluctuation ($J_4M_1S_1$ model). Concerning nitrogen-dependent couplings, see ref 31. [d] Coefficients (in Hz) for use with $^3J(\theta) = A \cos^2\theta + B \cos\theta + C$, else as footnote *c*.

**Table 3.** Substituent-Dependent $\chi_1$-Related Incremental Karplus Coefficients $\Delta C_0$ (Hz) As Inferred from Self-Consistent *J* Coupling Analysis[a]

| substituent type | substituent site | substituent[b] | $\Delta C_{0,\mathrm{rigid}}$ | $\Delta C_{0,\mathrm{Gauss}}$ | $\Delta C_{0,\mathrm{staggered}}$ | $\Delta J_0{}^{\mathrm{R}}$ [c] |
|---|---|---|---|---|---|---|
| inner/central | $C^\alpha$, $C^\beta$ | H → C | −0.49 | **−0.61** | −0.38 | −0.3 |
| | $C^\alpha$, $C^\beta$ | H → N[d] | ±0.00 | **±0.00** | ±0.00 | na |
| | $C^\alpha$, $C^\beta$ | H → O | −1.50 | **−1.59** | −1.30 | −0.9 |
| | $C^\alpha$, $C^\beta$ | H → S | −1.21 | **−1.30** | −1.10 | na |
| outer/terminal | N′, C′, $C^\gamma$ | H → C | −0.16 | **−0.16** | −0.01 | 0.3 |
| | N′, C′, $C^\gamma$ | H → N | +2.36 | **+1.81** | +1.90 | na |
| | N′, C′, $C^\gamma$ | H → O | +0.52 | **+0.61** | +0.76 | na |

[a] Component couplings shared among all amino acid and J coupling types and to be added to fundamental Karplus coefficients obtained from the same analysis using appropriate weights (see Supporting Information). Comparison for different models of local angular motion as indicated. Bolded values from the $J_4M_1S_1$ model were used to compile amino-acid-specific Karplus curves as given in Table 2. [b] Heavy-atom types are substituted for the default atom type H bonded to central ($C^\alpha$ or $C^\beta$) and terminal (N′, C′, or $C^\gamma$) positions, respectively. [c] Coupling increments referring to C,C three-bond coupling paths as taken from Table 7 in ref 33. Also see reviews of ref 34 and cited literature. [d] Parameter constrained at 0 for technical reasons, as the uniform N-substituent pattern at $C^\alpha$ of all standard amino acid types does not presently allow for discrimination of the effect.

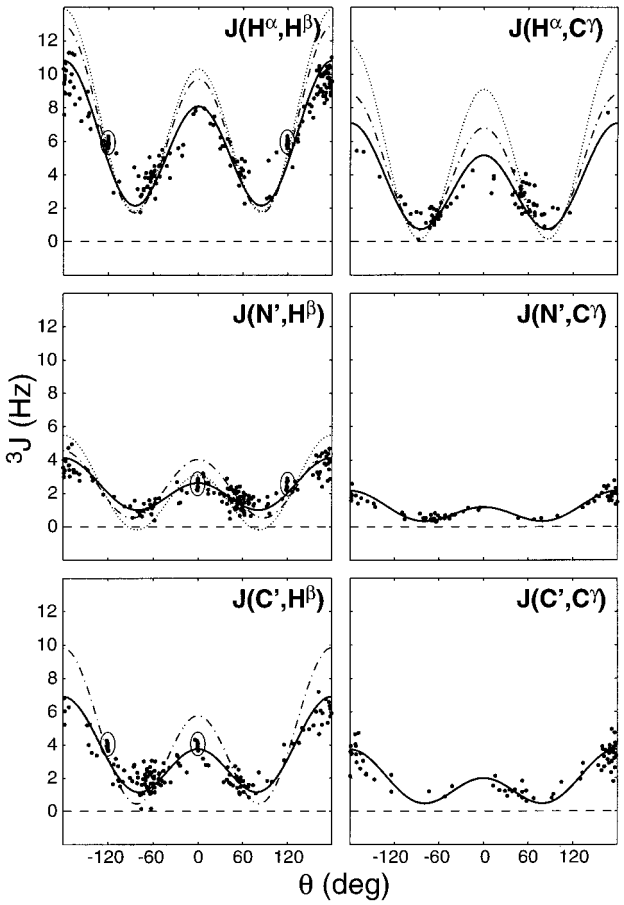


**Figure 3.** Self-consistent angular dependence of polypeptide $\chi_1$-related $^3J$ coupling constants. Dots indicate experimental $^3J$ coupling constants in *D. vulgaris* flavodoxin (alanine data encircled) plotted against optimized torsion angles from Table 4, including phase shifts to conform with geometric positions given in Figure 1. Solid lines are consensus Karplus curves $J(\theta)$ from optimized coefficients from Table 2 inserted into eq 1. Comparison Karplus curves refs 15−17 (dash−dotted) and refs 14, 19, and 37 (dotted). See text for details.

$\mathrm{RMSD}_J = 0.40$ Hz, half the error obtained with conventional Karplus parametrization procedures. Given in Table 2 is a set of consensus Karplus coefficients as calculated from residue-specific Karplus coefficients weighted by the amino acid composition in the fit. Representative of all amino acid types, consensus Karplus curves are those depicted in connection with experimental data in Figure 3. Henceforth, self-consistent results are based on the 249-variable fit, referring to at least four experimental *J* coupling constraints per residue and including topology and mobility effects ($J_4M_1S_1$).

**Statistical Significance of the New Karplus Parameters.** The RMS difference between fitted and experimental data is likely to decrease with an increased number of fit parameters in the optimization. In all self-consistent models, $J_4M_0S_0$ through $J_4M_1S_2$, the numbers of fit parameters are considerably larger than those in the X-ray-based conventional parametrization, i.e., from 130 to 249 as opposed to 18, respectively. This requires a statistically sound justification of the inclusion of additional adjustable parameters. In the framework of *F*-statistics, any two fit results can be compared on a *relative* basis by forming variance ratios between the residual fit errors, in comparison with associated numbers of degrees of freedom. In a statistical sense, both models differ significantly for low probabilities delivered. These probabilities of likelihood are shown as off-diagonal elements in the comparison matrix in Table 1. Comparison of the results from conventional Karplus parametrization with those from the most simple self-consistent model $J_4M_0S_0$ yields a vanishingly small probability, placing precedence on the self-consistent model, because of the more than 2-fold higher $\epsilon_J{}^2$ variance obtained in X-ray-based procedures when numbers of degrees of freedom are comparable. The larger number of experimental constraints in self-consistent fitting, partly making up for the loss of degrees of freedom, is due to the inclusion of additional alanine couplings, which is impossible with the conventional parametrization. Similarly, the initial self-consistent model $J_4M_0S_0$ and the best fit as of $J_4M_1S_1$ are significantly different, too. Although the number of fit parameters doubled, preference for the latter model arises from another great improvement in the fit error, comfortably compensating for the moderate decrease in the number of degrees of freedom.

Direct comparison of residual fit errors, normalized using the experimental standard error, and numbers of degrees of freedom gives rise to the *absolute* significance, as tested in the context of $\chi^2$ statistics. Derived from such probabilities are the acceptance measures given on the diagonal in the comparison matrix in Table 1. Only those self-consistent models which account for substituent effects show a certain statistical relevance. All the other models, including X-ray-based parametrizations, exhibit so low a probability that the result might be a chance event. Admittedly, such interpretation depends on the choice of the experimental standard error, set at $\sigma_J = 0.5$ Hz here, variation of which would affect the whole set of absolute probabilities, yet not the relative ranking of the models.

**Comparison with Previous Karplus Parametrizations.** To quantitate substituent effects, we refrained from applying the concept of generalized Karplus parameters devised by Altona and co-workers,[36] mainly because coefficients are available only for homonuclear proton−proton couplings. Primarily derived from cyclically constrained compounds, these sets involve up

to seven coefficients per coupling type, perhaps the reason generalized Karplus parameters have not become an integral part of standard biomolecular structure determination protocols, except for studies on proline and oligonucleotide conformation. To promote acceptance of any newly derived parameter set, it has been paramount to the present approach *not to increase* the number of Karplus coefficients needed with a specified $J$ coupling type, a prerequisite fulfilled by the proposed concept of fundamental and incremental Karplus coefficients.

Consensus Karplus coefficients of Table 2 can be compared with parameters commonly referred to when interpreting $\chi_1$-related $^3J$ couplings (Figure 3). The average $J$ coupling discrepancy incurred by either of two sets of Karplus parameters is determined from the difference in their coefficients, as given by

$$\Delta J_{\mathrm{rms}} = \{(\Delta C_0)^2 + 0.5(\Delta C_1)^2 + 0.5(\Delta C_2)^2\}^{1/2} \qquad (4)$$

for the Fourier representation of the dihedral angle dependence according to eq 1, or alternatively, by $\Delta J_{\mathrm{rms}} = \{0.375(\Delta A)^2 + 0.5(\Delta B)^2 + (\Delta C)^2 + \Delta A \Delta C\}^{1/2}$ for the cosine power representation.[3] Accordingly, expected $J$ discrepancies averaged for the revolving torsion between our coefficients and those given for $^3J_{\mathrm{H}\alpha,\mathrm{H}\beta}$,[15] $^3J_{\mathrm{N}',\mathrm{H}\beta}$,[16] $^3J_{\mathrm{C}',\mathrm{H}\beta}$,[16] and $^3J_{\mathrm{H}\alpha,\mathrm{C}\gamma}$[17] are 0.96, 0.62, 1.27, and 1.34 Hz, respectively. Earlier $^3J_{\mathrm{H}\alpha,\mathrm{H}\beta}$ coefficients[14,18] produce average coupling discrepancies of 1.47 and 0.79 Hz, while alternative $^3J_{\mathrm{N}',\mathrm{H}\beta}$ coefficients[19] give 0.71 Hz. Comparison $^3J_{\mathrm{H}\alpha,\mathrm{C}\gamma}$ coefficients given derive from ab initio calculations on propane. Alternative parameters have been derived from the $\chi_2$-related $\mathrm{C}^\alpha-\mathrm{C}^\beta-\mathrm{C}^\gamma-\mathrm{H}^\gamma$ fragment in ornithine,[37] raising the discrepancy to as large as 2.88 Hz. Both latter sets refer to possibly inappropriate models of the $\mathrm{H}^\alpha-\mathrm{C}^\alpha-\mathrm{C}^\beta-\mathrm{C}^\gamma$ fragment in the common amino acid side chains. No comparison parametrizations of $^3J_{\mathrm{N}',\mathrm{C}\gamma}$ and $^3J_{\mathrm{C}',\mathrm{C}\gamma}$ couplings are available thus far.[1,22]

**Cross Validation of the New Karplus Parameters Using X-ray Reference Torsions.** Given the amino-acid-specific Karplus parameters obtained with the best-fit model $J_4M_1S_1$, $J$ coupling constants predicted according to eq 3 for the flavodoxin X-ray reference conformation[28] differed from experimental values by only 0.64 Hz on average, while traditional Karplus parameters[15−17] combined with X-ray torsion angles yielded a $\mathrm{RMSD}_J$ of 1.84 Hz. This is not surprising, if the various Karplus curves displayed in Figure 3 are compared, and in fact, the result was expected from the measure given in eq 4, too. To be fair, such comparison was restricted to those 76 residues whose NMR- and X-ray-derived torsion angles agreed within ±30°, and also ignored coupling types $^3J_{\mathrm{N}',\mathrm{C}\gamma}$ and $^3J_{\mathrm{C}',\mathrm{C}\gamma}$, for which no comparison parametrizations are available. Predictions of $^3J_{\mathrm{H}\alpha,\mathrm{H}\beta}$ and $^3J_{\mathrm{C}',\mathrm{H}\beta}$, among those couplings most conveniently measured in $\chi_1$ angle determination, were found to be particularly sensitive to variations in the Karplus parameters used. Arguably, Gaussian distribution profiles imposed on angles in the fit $J_4M_1S_1$ may not be valid in connection with X-ray angles. However, trends were similar for rigid X-ray torsions, too, giving $J$ coupling discrepancies of 0.70 and 1.76 Hz with self-consistent Karplus parameters as of $J_4M_0S_1$ ($\sigma_\theta = 0$) and with traditional ones, respectively. Finally, the comparison might ignore effects from substituents and mobility altogether, and, applying the simpler eq 1 to X-ray-derived reference torsion angles, the basic self-consistent Karplus parameters as of $J_4M_0S_0$ ($\sigma_\theta = 0$, $\Delta C_0 = 0$) would yield an average $J$ coupling discrepancy of 0.78 Hz, which increased at 1.77 Hz when using conventional Karplus parameters. Interestingly, consensus Karplus parameters as of $J_4M_1S_1$, which per se do not account for mobility or topology effects, gave only a moderate fit of 0.95 Hz average violation between experimental $J$ coupling constants and those calculated for $\chi_1$ torsions from the X-ray dataset.

**Comparison of *D. vulgaris* Flavodoxin $\chi_1$ Conformations in NMR and X-ray Structures.** Self-consistent $\chi_1$ torsions obtained from the best-fit model ($J_4M_1S_1$) are given in Table 4. Accounting for one-quarter of the total square error ($\epsilon_J^2 = 500.2$) are those nine residues which violated the $J$ coupling constraints most (respective error fractions given in parentheses), including Phe91 (4.9%), Trp60 (3.6%), Asp143 (2.8%), Phe47 (2.4%), Glu109 (2.3%), Tyr17 (2.3%), Asp34 (2.1%), Asp51 (2.0%), and Tyr31 (2.0%). Other residues comply with experimental data such as to contribute less than 2% each to the error sum. Matching the experiment within 1, 2, and 3 standard error units of $\sigma_J = 0.5$ Hz were 562, 136, and 14 $J$ coupling constants, respectively, out of 713 total considered (excluding duplicate alanine entries). No constraint violation exceeded 2.0 Hz in the final converged dataset (see Supporting Information). A single outlier exceeded the $3\sigma$ interval, namely $^3J_{\mathrm{H}\alpha,\mathrm{C}\gamma}$ in Phe91, a side chain for which other $J$ coupling constraints could be established mainly as semiquantitative upper limits from the absence of cross-peaks in $J$-correlated spectroscopy. Similarly, weak NMR multiplets from Trp60 and Asp143 might have introduced experimental uncertainty. However, rotamer geometries obtained, respectively around +60°, −60°, and −60°, agree well with X-ray reference data.

Although reference is made to the crystal structure of the wild-type flavodoxin,[28] it is important to reiterate that X-ray data do not control the self-consistent NMR data evaluation at any stage. Applying a tolerance of ±30°, $\chi_1$ orientations of approximately 80% of the rotatable amino acid side chains in flavodoxin agree with X-ray reference data (Figure 4). Yet, this leaves a considerable portion of the molecule to be looked at in more detail. With regard to torsion angle discrepancy, topping the list were 18 out of the 95 non-alanine residues (deviation in degrees given in parentheses), including Ser97 (176.4), Asp63 (172.2), Glu99 (153.3), Pro73 (149.9), Asp69 (101.5), Lys3 (100.4), Glu110 (77.2), Arg24 (68.2), Asp62 (58.8), Glu20 (48.7), Val88 (46.7), Asp34 (40.3), Glu118 (40.3), Leu67 (38.2), Ile148 (37.4), Ser35 (33.9), Glu42 (32.1), and Ser10 (31.0).

An artifact from the self-consistent optimization procedure itself is excluded on the grounds that the very same method proved successful in the refinement of flavodoxin $\phi$ torsion angles, where NMR and X-ray results agreed surprisingly well.[8] Furthermore, it was insignificant for improving the overall fit temporarily to exclude from the calculations data of those side chains whose orientation substantially deviated from X-ray conformations, because only about average $J$ discrepancies were removed then. On the contrary, half of the 18 side chains exhibiting $\chi_1$ conformations different from X-ray data comfortably fitted all experimental $J$ coupling constraints within one standard error unit of $\sigma_J = 0.5$ Hz (see Supporting Information). As the majority of these residues comes with numerous coupling constraints, often up to the maximum nine values, or six with serines, disagreement with reference torsions hints at genuine differences between NMR- and X-ray-based molecular models. Most revealing, perhaps, apart from residue Asp34, there is no

(36) (a) Haasnoot, C. A. G.; de Leeuw, F. A. A. M.; Altona, C. *Tetrahedron* **1980**, *36*, 2783−2792. (b) Haasnoot, C. A. G.; De Leeuw, F. A. A. M.; de Leeuw, H. P. M.; Altona, C. *Org. Magn. Reson.* **1981**, *15*, 43−52. (c) Haasnoot, C. A. G.; De Leeuw, F. A. A. M.; de Leeuw, H. P. M.; Altona, C. *Biopolymers* **1981**, *20*, 1211−1245. (d) De Leeuw, F. A. A. M.; Altona, C. *Int. J. Pept. Res.* **1982**, *20*, 120−125.

(37) DeMarco, A.; Llinás, M. *Biochemistry* **1979**, *18*, 3846−3854.

**Table 4.** Optimized Side-Chain Torsion Angles $\chi_1$ (deg) in *Desulfovibrio vulgaris* Flavodoxin As Inferred from Self-Consistent *J* Coupling Analysis[a]

| | NMR[c] | X-ray[d] | | | | NMR | X-ray | | |
|---|---|---|---|---|---|---|---|---|---|
| residue[b] | $J_4M_1S_1$ ($\chi_1 + \sigma_{\chi 1}$) | Walsh | 2FX2 | 3FX2 | residue | $J_4M_1S_1$ ($\chi_1 \pm \sigma_{\chi 1}$) | Walsh | 2FX2 | 3FX2 |
| Pro-2 | −4.2 ± 0.2 | −5.4 | na | na | Phe-71 | −147.9 ± 0.1 | −153.9 | −151.8 | −152.0 |
| Lys-3 | * −38.4 ± 32.5 | −138.8† | −88.9 | −50.5† | Ile-72 | 173.5 ± 0.2 | −179.8 | 172.2 | 168.9 |
| Leu-5 | −178.2 ± 19.9 | 170.9 | −168.8 | 177.8 | Pro-73 | * 135.9 ± 13.4 | −14.0 | −14.4 | −15.9 |
| Ile-6 | −177.9 ± 14.6 | 176.2 | 168.1 | 176.6 | Leu-74 | 159.0 ± 12.5 | 174.0 | 174.1 | 170.4 |
| Val-7 | −178.5 ± 25.1 | −171.7 | −172.5 | −171.8 | Phe-75 | 172.2 ± 18.7 | −179.0 | −176.3 | −176.8 |
| Ser-10 | * 162.9 ± 22.4 | −166.1 | −163.7 | −166.2 | Ser-77 | −58.8 ± 39.5 | −64.5 | −74.8 | −58.3 |
| Thr-12 | −38.0 ± 29.0 | −48.1 | −49.7 | −52.7 | Leu-78 | −109.6 ± 44.1 | −87.2 | −125.5 | −76.1 |
| Asn-14 | −63.6 ± 24.7 | −73.8 | −69.9 | −86.4 | Glu-80 | * −63.8 ± 22.0 | −33.7 | −82.0† | 77.0‡ |
| Thr-15 | −156.5 ± 25.6 | −174.3 | −179.6 | −172.8 | Thr-81 | −77.7 ± 23.8 | −66.5 | −70.7 | −57.5 |
| Glu-16 | 177.7 ± 27.7 | −179.4 | 179.9 | 179.6 | Gln-84 | 155.3 ± 31.7 | 155.4 | −177.3 | 143.3 |
| Tyr-17 | 152.2 ± 16.0 | 162.6 | 164.6 | 162.2 | Arg-86 | −145.8 ± 40.6 | −173.9 | −162.0 | −163.2 |
| Thr-18 | −169.2 ± 0.1 | −175.9 | −176.9 | 163.0 | Lys-87 | −64.6 ± 0.1 | −89.0 | −82.0 | −70.3 |
| Glu-20 | * −27.1 ± 32.4 | −75.8 | −72.4 | −75.2 | Val-88 | * 133.7 ± 25.8 | −179.6‡ | −59.0 | −56.5 |
| Thr-21 | −164.6 ± 20.7 | −177.4 | −176.7 | 178.1 | Phe-91 | 46.9 ± 19.0 | 57.2 | 54.2 | 62.1 |
| Ile-22 | 173.3 ± 15.0 | 172.4 | 173.8 | 167.5 | Cys-93 | −56.5 ± 11.1 | −68.4 | −80.1 | −71.8 |
| Arg-24 | * 141.4 ± 17.0 | −150.4 | 172.6 | 169.5 | Ser-96 | 62.3 ± 21.0 | 59.8 | 60.4 | 54.6 |
| Glu-25 | −85.6 ± 41.7 | −70.9 | −74.6 | −85.4 | Ser-97 | *−113.2 ± 0.0 | 70.4 | 71.8 | 83.5 |
| Leu-26 | −72.9 ± 0.2 | −96.4 | −66.4 | −72.0 | Tyr-98 | −71.2 ± 22.4 | −66.3 | −71.8 | −64.1 |
| Asp-28 | −80.1 ± 28.3 | −76.9 | −85.3 | −67.1 | Glu-99 | * −6.8 ± 16.9 | −160.1 | 146.0† | −164.4 |
| Tyr-31 | −81.2 ± 23.0 | −77.4 | −80.9 | −87.6 | Tyr-100 | −51.1 ± 26.9 | −52.0 | −56.5 | −30.3 |
| Glu-32 | −4.2 ± 15.4 | −7.3† | −64.3 | −72.3 | Phe-101 | 162.2 ± 0.0 | 168.2 | 172.2 | 178.8 |
| Val-33 | 172.5 ± 27.8 | −179.7 | 175.5 | 179.7 | Cys-102 | −75.6 ± 17.1 | −77.1 | −79.5 | −79.2 |
| Asp-34 | * 167.6 ± 29.7 | −152.1 | −168.5 | −175.9 | Val-105 | 170.1 ± 15.8 | −179.2 | −170.2 | −172.1 |
| Ser-35 | * 149.2 ± 22.4 | −176.9 | −167.4 | −147.9 | Ile-108 | 177.2 ± 16.1 | 173.2 | −177.1 | 178.7 |
| Arg-36 | −45.7 ± 0.2 | −61.2 | −56.7 | −43.4 | Glu-109 | −68.4 ± 22.5 | −73.3 | −72.6 | −40.9 |
| Ser-40 | 98.3 ± 26.1 | 76.7 | 85.8 | 82.8 | Glu-110 | * 149.3 ± 26.6 | −133.5 | −146.9 | −167.4 |
| Val-41 | −51.6 ± 24.7 | −53.2 | −51.6 | −29.9 | Lys-111 | 178.3 ± 34.4 | −180.0 | −176.3 | 179.9 |
| Glu-42 | * −46.1 ± 28.7 | −78.2 | −93.2 | −44.4 | Leu-112 | −75.8 ± 8.4 | −73.4 | −104.7 | −79.8 |
| Leu-46 | 179.9 ± 27.3 | −178.2 | 179.1 | 172.7 | Asn-114 | −51.9 ± 29.6 | −71.1 | −67.4 | −59.9 |
| Phe-47 | −52.5 ± 0.2 | −56.9 | −49.5 | −46.9 | Leu-115 | −63.2 ± 29.2 | −74.8 | −84.4 | −81.3 |
| Phe-50 | −78.0 ± 0.8 | −76.5 | −77.3 | −59.3 | Glu-118 | * 139.8 ± 12.6 | −179.9 | −170.3 | 173.2 |
| Asp-51 | −48.4 ± 0.0 | −57.5 | −54.3 | −59.8 | Ile-119 | −177.5 ± 0.3 | 177.0 | 171.6 | −177.7 |
| Val-53 | 169.3 ± 21.7 | 176.0 | 177.3 | 167.5 | Val-120 | −42.3 ± 25.5 | −53.6 | −53.0 | −53.7 |
| Leu-54 | −59.9 ± 23.2 | −65.8 | −68.9 | −52.8 | Asp-122 | −58.8 ± 27.2 | −62.0 | −71.7† | 41.6‡ |
| Leu-55 | −77.3 ± 0.1 | −64.2 | −99.6 | −67.6 | Leu-124 | 165.2 ± 15.6 | 177.8 | 175.9 | 173.7 |
| Cys-57 | −144.0 ± 20.3 | −171.4 | −175.4 | −171.0 | Arg-125 | −79.6 ± 20.9 | −70.6 | −70.4 | −69.0 |
| Ser-58 | 57.4 ± 31.8 | 45.4 | 52.1 | 36.2 | Ile-126 | 172.5 ± 11.0 | 179.1 | 175.6 | 176.4 |
| Thr-59 | 177.6 ± 17.1 | −173.6 | −165.4 | −161.1 | Asp-127 | 176.0 ± 13.7 | −172.6 | 179.6 | −174.3 |
| Trp-60 | −65.3 ± 30.7 | −68.9 | −64.8 | −69.7 | Arg-131 | −64.0 ± 17.5 | −60.2 | −58.4 | −53.4 |
| Asp-62 | * 127.7 ± 0.1 | −173.5 | −176.8 | 176.5 | Arg-134 | −172.1 ± 30.8 | −161.2 | −169.4 | −170.7 |
| Asp-63 | *−134.9 ± 48.6 | 52.9 | 78.8 | 66.7 | Asp-136 | −62.9 ± 17.1 | −69.7 | −66.5 | −79.1 |
| Ser-64 | 54.6 ± 30.7 | 65.7 | 68.6 | 68.6 | Ile-137 | 178.9 ± 0.0 | 173.7 | −178.7 | 177.2 |
| Ile-65 | 169.1 ± 33.9 | 168.3 | 166.6 | 173.9 | Val-138 | 167.0 ± 22.3 | 168.4 | 163.7 | 166.0 |
| Glu-66 | −68.0 ± 28.4 | −50.6 | −51.7 | −27.8 | Asp-143 | −67.4 ± 28.0 | −66.4 | −56.4 | −48.4 |
| Leu-67 | * −59.1 ± 27.7 | −97.3 | −93.0 | −102.9 | Val-144 | 133.5 ± 30.7 | 162.6‡ | −38.1† | −54.5 |
| Gln-68 | −177.2 ± 33.7 | −166.5 | −163.1 | −173.3 | Arg-145 | −106.0 ± 13.1 | −78.2 | −83.9 | −82.6 |
| Asp-69 | * −69.9 ± 32.7 | −171.4 | 55.0‡ | 177.7 | Ile-148 | * −20.4 ± 28.8 | −57.8 | −64.9 | −73.6 |
| Asp-70 | −52.8 ± 0.0 | −61.0 | −61.5 | −72.1 | | | | | |

[a] The torsion angle path strictly follows the scheme outlined in Figure 1, according to which isoleucine and threonine angles in both NMR and X-ray conformations are consistently taken from $C^{\gamma 2}$ to unify phase shifts; see text. [b] Excludes Tyr8, Asp37, Glu48, Leu52, Asp76, Glu79, Cys90, Asp95, Asp106, Lys113, Gln121, Pro130, Asp135, Trp140, and His142, for which degenerate H$\beta$ proton resonances impede torsion angle determination on the basis of less than four coupling constants. [c] Torsion angles from the best-fit self-consistent *J* coupling model using a minimum four coupling constants per residue, including Gaussian angular fluctuation and substituent effects (6 × 3 fundamental plus 7 incremental Karplus coefficients). Values marked by asterisks deviate by more than 30° from torsions in the X-ray reference set "Walsh". [d] Torsion angles from X-ray diffraction data. "Walsh" denotes the structure of the wild-type *D. vulgaris* flavodoxin-FMN complex (oxidized) resolved at 0.17 nm by Dr. Martin Walsh (EMBL-Hamburg, personal communication). Coordinate sets 2FX2 and 3FX2 (PDB) of the $Pro^2Ala$ mutant protein from data collected at ambient temperature and 123 K were both resolved at 0.19 nm and refined with *R* factors of 0.17 and 0.20, respectively, according to ref 27. Single and double daggers mark entries which deviate from the average formed by the three datasets by more than 30° and 60°, respectively.

overlap between the two groups of residues short-listed above, allowing us to conclude that violations in *J* and $\chi_1$ are virtually uncorrelated, underscoring the possibility of truly different local structure under NMR and X-ray conditions.

Subject to substantial conformational averaging in solution and possibly prone to packing artifacts in the crystal, side chains on the protein surface might occasionally lock into different orientations under both NMR and X-ray experiment conditions. Out of those 18 side chains with disagreeing $\chi_1$ conformations, 15 were indeed found to be solvent exposed (Figure 4), and, according to our analysis, they are likely to be flexible above average, too. The exceptions were Ser10 pointing at the phosphate group of the FMN-ribityl moiety, Pro73 located in a helical arrangement, and Val88 oriented toward the protein core.

Some torsion angles fitted showed dependence on the absence or presence of mobility (Asp62 and Val88) or substituent effects (Glu99 and Ser97) in the model. In Val88, problems may have also arisen from degenerate $C^{\gamma}$ resonances, preventing $^3J_{N'C\gamma}$ and $^3J_{C'C\gamma}$ from being collected. Rather than lack of data, numerical ambiguity of the kind discussed in the context of

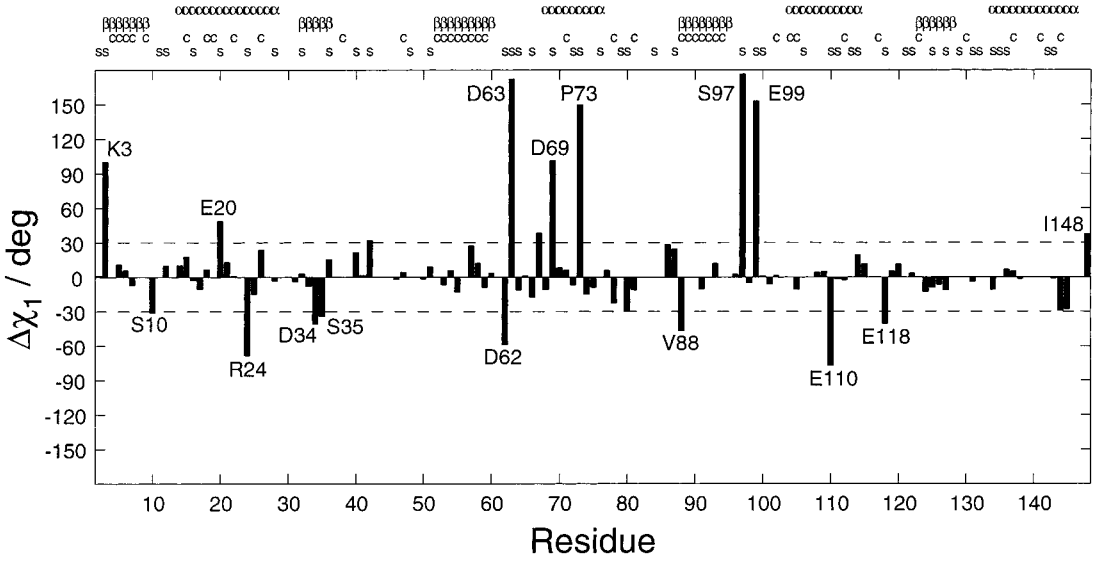


**Figure 4.** Differences between side-chain torsion angles $\chi_1$ in *D. vulgaris* flavodoxin as obtained from self-consistent *J* coupling analysis and those taken from X-ray coordinates.[28] Results are given for the model $J_4M_1S_1$, including mobility and substituent effects. Respective symbols indicate residues involved in α helix or $\beta$ sheet secondary structure according to previous NMR investigations. Residues are marked "c" and "s", depending on whether they are completely buried in the protein core or are partly surface exposed in the reference X-ray coordinate set.[38]

backbone torsions, $\phi$,[3] was responsible for an unexpected approximately 180° flip of $\chi_1$ in the Pro73 side chain with endocyclic torsions topologically confined to a range of $\chi_1 = 0 \pm 40°$ normally. Comparison with more sensible results for Pro2 in the same analysis hints at the subtle (numerical) propensity of NMR-derived torsion angles occasionally to accommodate degenerate states owing to the multivalued Karplus relation.

With regard to Asp34 and Ser10, both NMR and X-ray side-chain conformations were found to be distorted from the $\chi_1 = 180°$ rotamer, in opposite directions though. The mobility models fitted, both Gaussian random fluctuation and three-site jump, suggest only moderate angular flexibility in these side chains, claiming the presence of a single predominant rotamer ($p_2 > 60\%$). Interestingly, statistics on X-ray diffraction data do supply evidence for systematic variation of mean torsion angles in polypeptide side chains with resolution.[39] Accordingly, "skewed" dihedral angle conformations and concomitant low *B* factors, in particular in gauche arrangements, seem to be the rule rather than the exception. Such phenomena help explain the divergent Karplus parameter sets obtained for $\chi_1$-dependent amino acid side-chain couplings following the conventional calibration method on the basis of X-ray reference geometries.

Unambiguous stereospecific resonance assignments emerged for all 80 susceptible side chains included in the self-consistent analysis, except those experiencing the most extensive angular averaging, as there are Asp63, Ser77, and Leu78. Stereospecific assignments varied with the model applied, as Gaussian distributions exceeded widths of ±40°, producing similar fit errors with either possible mapping (see Supporting Information). It has been only recently that dynamic information in crystal structure datasets has been scrutinized.[39,40] Interestingly, X-ray data for Lys3, Glu32, Asp69, Glu80, Val88, Asp122, and Val144 (as well as Glu79 and Lys113 not contained in the present analysis) exhibit at least one stray value among the three available torsion orientations (Table 4), considering $\chi_1$ to deviate by more than 30° from the average and the standard deviation to exceed 30° in those sets. Respective $\gamma$ positions also indicate elevated *B* factors of more than twice the magnitude typically found for backbone atoms. Interestingly, most of these disordered residues are located on the protein surface (Figure 4). At the present sophistication levels of the mobility models employed in the NMR analysis, self-consistent *J* coupling analysis does support conformational flexibility in all these residues, too. For example, NMR-derived conformations of Lys3 and Glu80 would agree with the earlier flavodoxin coordinate sets 2FX2 and 3FX2, and Gaussian libration and staggered rotamer models (see Supporting Information) reveal broad $\chi_1$ angle distributions (Lys3, Asp69, Glu80, and Asp122) and two-site equilibria (Glu32, Val88, and Val144). Yet, correlation of crystallographic *B* factors and NMR mobility parameters looks rather weak (Figure 5),[42] because dynamics parameters are subject to totally different averaging processes in the two methods, making a clear-cut distinction as to which angular motion model applies best in each case extremely difficult.

## Discussion

**Properties of the Self-Consistent *J* Coupling Models.** When determining amino acid side-chain dihedral angles $\chi_1$ on the basis of $^3J$ coupling information, both conformational averaging and substituent effects play a critical part in the data interpretation process. This contrasts with studies on polypeptide backbone torsions $\phi$, where both angular flexibility and topology variation are usually of minor concern. $^3J$ couplings undoubtedly depend on the dihedral angle orientation in the first place. However, mobility and topology effects compound the fundamental torsion angle dependence, such that—in the present work—the observable coupling constant $J_{obs} = J_{torsion} + J_{mobility} + J_{topology}$. Likewise, the overall fit error factorizes into variances, associated with the intrinsic contributions, and an additional random component, as given by $\epsilon_J^2 = \epsilon_{J,torsion}^2 +$

(38) (a) Lee, B.; Richards, F. M. *J. Mol. Biol.* **1971**, *55*, 379−400. (b) Hubbard, S. J.; Campbell, S. F.; Janet, J. M. *J. Mol. Biol.* **1991**, *220*, 507−530. (c) Hubbard, S. J.; Janet, J. M. NACCESS, Computer Program, Department of Biochemistry and Molecular Biology, University College of London.

(39) MacArthur, M. W.; Thornton, J. M. *Acta Crystallogr., Sect. D: Biol. Crystallogr.* **1999**, *55*, 994−1004.

(40) Carugo, O.; Argos, P. *Protein Eng.* **1997**, 10, 777−787.

(41) (a) Janin, J.; Wodak, S.; Levitt, M.; Maigret, B. *J. Mol. Biol.* **1978**, *125*, 357−386. (b) Ponder, J. W.; Richards, F. M. *J. Mol. Biol.* **1987**, *193*, 775−791.

(42) MacArthur, M. W.; Thornton, J. M. *Proteins* **1993**, *17*, 232−251.

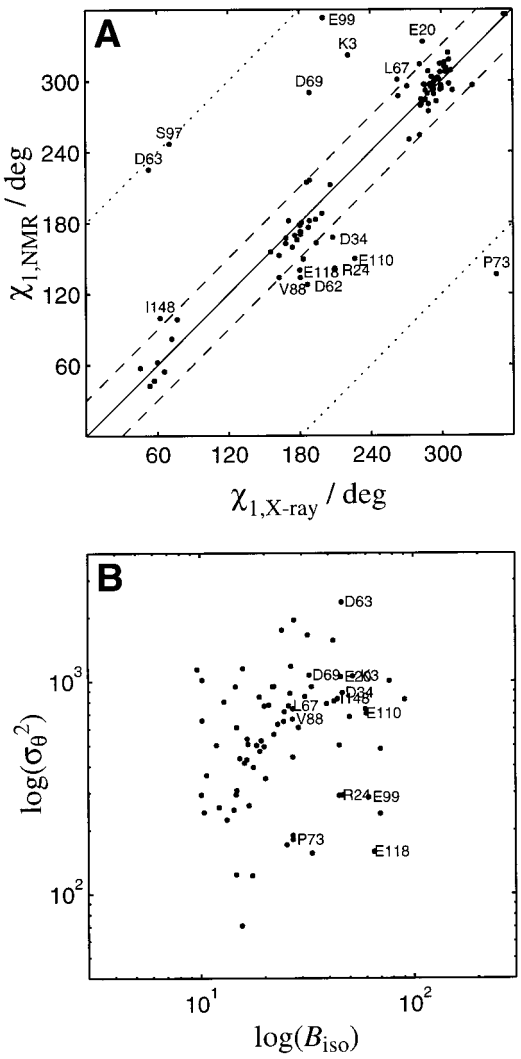


**Figure 5.** Comparison of static and dynamic properties of *D. vulgaris* flavodoxin side-chain $\chi_1$ torsions as inferred from crystallographic data by Walsh[28] and self-consistent *J* coupling analysis using model $J_4M_1S_1$ including mobility and substituent effects. (A) Correlation of *J* coupling and X-ray-derived $\chi_1$ torsions showing most of the side-chain orientations to agree within a tolerance of ±30° (dashed lines). Torsions deviating by more than 40° from X-ray data are labeled. Discrepancies of about 180° (dotted lines) are due to numerical ambiguity as discussed in the text. Comparison of isoleucine and threonine torsion angles necessitated reversing phase shifts applied during computations of the present work. Staggered rotamer populations agree with probability profiles from databank statistics.[41] (B) Correlation between angular variance, $\sigma_\theta^2$, as obtained from *J* coupling analysis, and isotropic thermal factors of $\gamma$ atoms, $B_{iso}$, as given with the X-ray dataset. Note the log scales. Like in panel A, residue labels indicate disagreement between NMR and X-ray static $\chi_1$ conformations (Asp62 and Ser97 exhibit nearly zero fluctuation in the NMR analysis). Interestingly, all the residues highlighted exhibit above average thermal disorder in the X-ray dataset.

$\epsilon^2_{J,\text{topology}} + \epsilon^2_{J,\text{random}}$. The challenge is to separate all the possible contributions unambiguously.

The various factors might mutually conceal each other because iterative modeling necessarily results in a compromise solution. The host of substituents in different amino acid types causes a spread of coupling constants for like dihedral angle conformations and, when using conventional calibration methods, inevitably translates into a more shallow underlying Karplus curve, as has been shown for angular mobility.[10,24] While Figure 2 is proof that substituent effects are indeed prominent in *J*-coupling-based modeling of side-chain angles $\chi_1$ in *D. vulgaris* flavodoxin, error gauges in Table 1 hint at considerable angular mobility being present in addition.

In this study, interference between both mobility and topology effects is excluded by way of implementation in the model. Basically, partition of the effects is guaranteed by the distinct numerical properties of the model constituents. Mobility invariably associates with the angle-dependent portion of the observed *J* couplings, leaving unaltered the rotationally averaged coupling reflected in the Karplus coefficients $C_0$. Mobility effects necessarily feed through to $C_1$ and $C_2$ coefficients. In contrast, substituent-related variables have been rationalized to modulate the angle-independent portion of the Karplus relation only; i.e., they affect coefficients $C_0$, but not $C_1$ or $C_2$. The simulations indeed showed barely varying $C_0$ coefficients in optimizations including and excluding angular mobility, whereas coefficients $C_1$ and $C_2$ consistently adopted smaller and larger absolute values in both mobility models ($M_{1,2}$) as compared to the rigid situation ($M_0$). By the same token, the average mobility of $\chi_1$ torsions turned out to be virtually uniform in the absence and presence of substituent effects; i.e., $\langle\sigma_\theta\rangle = 23.2°$ and 24.4° in optimizations $J_4M_1S_0$ and $J_4M_1S_1$, respectively. Investigations relying on conventional Karplus parametrization strategies revealed $\langle\sigma_\theta\rangle = 26°$.[43] Importantly, it is concluded that accounting for substituent effects in $^3J$-based structure refinement does not reduce the scope for potential mobility, and vice versa.

**Implications to Molecular Structure Determination.** Neglecting substituent effects raises the risk of misinterpreting the $\chi_1$ torsion angle conformation in the context of the staggered rotamer analysis.[44] This is exemplified by the amino-acid-dependent swings in predicted trans and gauche couplings (Table 2), being as large as 1.0−2.5 Hz, in excellent agreement with the ranges seen in experimental data.[2] Most dependent on topology are those *J* coupling types involving the $H^\alpha$ proton, owing to the large proton gyromagnetic ratio used for normalizing incremental effects.

Somewhat counterintuitive, experimental $^3J_{C',C\gamma}$ and $^3J_{N',C\gamma}$ values are commonly found to be above average in those aromatic side chains for which our amino-acid-specific Karplus curves predict respective $J_{trans}$ and $J_{gauche}$ values to be among the smallest. This implies in turn that either, on average, $C^\gamma$-related trans couplings reach the top of the Karplus curve sooner with phenylalanine, tyrosine, and tryptophane than with other amino acid types, or inversely, conformations of these side chains are already nearly perfect staggered states with only little angular fluctuation,[45] deceptively showing intermediate $^3J$ values typical of mobile side chains otherwise. While $^3J_{C',C\gamma}$ and $^3J_{N',C\gamma}$ coupling constants take maximum values in the two most abundant staggered conformations with $\chi_1 = -60°$ and 180°, respectively, too few coupling data are available as yet as to perceive amino acid type-sensitive phenomena with trans $^3J_{H\alpha,C\gamma}$ coupling constants, for the then required $\chi_1 = +60°$ rotamer is least abundant.

The opposite conclusion would be arrived at with residue types aspartic acid, asparagine, and presumably histidine, all of them containing $C^\gamma$-bound nitrogen and/or oxygen, connected with positive coupling increments. As incremental Karplus coefficients hint at the largest possible $C^\gamma$-related couplings for trans as well as gauche situations, these amino acids appear to stand out from the expected range of *J* values. Indeed, values

(43) West, N. J.; Smith, L. J. *J. Mol. Biol.* **1998**, *280*, 867−877.
(44) (a) Pachler, K. G. R. *Spectrochim. Acta* **1963**, *19*, 2085−2092. (b) Pachler, K. G. R. *Spectrochim. Acta* **1964**, *20*, 581−587.
(45) Hu, J.-S.; Grzesiek, S.; Bax, A. *J. Am. Chem. Soc.* **1997**, *119*, 1803−1804.

of $^3J_{N',C\gamma}$ and $^3J_{C',C\gamma}$ in Asx residues have been reported to exceed 3 and 5 Hz, respectively.[2,6,46] Given the concept developed here, the allegedly exceptional $^3J_{C',C\gamma}$ coupling constant of 5.1 Hz found for Asp95 in SNase[46] or 5.5 and 5.6 Hz measured for Asp21 and Asp58 in ubiquitin[2,6] turn out to be not that much of an exception any longer. Our results would not support the rationalization either that "the wide range of $^3J_{C',C\gamma}$ values cannot be related to $C^\gamma$ substituents because a similar dependence of $\phi$-related $^3J_{C',C\beta}$ couplings on $C^\beta$ substituents had not been observed",[2] simply because amino acid topology surrounding the backbone torsion is considerably more uniform. Predictions on the basis of amino-acid-specific Karplus curves are also consistent for valine and isoleucine side chains with multiple carbon substituents at the central $C^\beta$ connected with negative coupling increments.

## Concluding Remarks

The present results should facilitate the use of *J* coupling information in NMR-based molecular modeling. Unlike polypeptide backbone $\phi$ torsion refinement, quantitative determination of amino acid side-chain torsions $\chi_1$ needs to take into account effects from both angular mobility and variable topology. Variation in atomic substituent patterns in amino acids and the consequential scarcity of suitable reference compounds of known geometry make side-chain-related Karplus parameters harder to obtain than those related to backbone torsions. A novel and simple combination of fundamental and incremental Karplus parameters proved sufficient to resolve in the *J* coupling constants an angle-independent portion ascribed to substituents. Quantification of substituent effects in flavodoxin also enabled consistent interpretation of a range of amino acid side-chain coupling constants observed in other proteins.

The solution structure of *D. vulgaris* flavodoxin, refined in terms of side-chain $\chi_1$ torsions solely using $^3J$ coupling information, conforms with results from various X-ray studies. Remaining discrepancies between NMR- and X-ray-derived $\chi_1$ conformations are explained by genuine differences between solution and crystal structures and can be attributed to crystal-packing effects or conformational equilibria between multiple $\chi_1$ rotamers in both solution and the solid state.

The following assumptions were crucial to the feasibility of the present investigation into the substituent dependence of polypeptide side-chain $\chi_1$-related $^3J$ coupling constants: (i) Local geometries at $C^\alpha$ and $C^\beta$ sites are perfectly tetrahedral, allowing uniform phase increments to be used. (ii) The concept of component couplings implies that effects from mobility and topology are separable and additive, prerequisites ensured by the numerical implementation of the effects in the *J* coupling models. (iii) The average coupling magnitude, $C_0$, correlates with the gyromagnetic ratios of the actively coupled atom types, a fact used to normalize incremental interactions when being added to the various fundamental couplings.

At present, only corrections to rotation-invariant Karplus coefficients $C_0$ are statistically significant. Impossible though it may be at the current level of experimental data, future studies using larger *J* coupling datasets, conveying more uniform distribution both of amino acid type occurrence and of dihedral angle conformation, might explore more subtle substituent effects by using increments to angle-dependent Karplus parameters as well.

Not being dependent on supplementary information, self-consistent calibration of Karplus coefficients lives on data redundancy and parameter overdetermination, so that certain experimental $^3J$ coupling data, normally discarded in the absence of suitable Karplus parameters, can still be used to advantage. The method is expected to benefit from extensive future *J* coupling sets, not necessarily only that of a single protein. If acquired under similar conditions, co-refinement of *J* coupling datasets from two or more proteins will enable parameter assessments to be made on wider statistical grounds. The novel concepts are not limited to polypeptide couplings; application to saccharides and oligonucleotides is conceivable.

## Experimental Section

$^{15}$N-Singly and $^{13}$C,$^{15}$N-doubly enriched samples of recombinant wild-type *D. vulgaris* flavodoxin, expressed and purified as described elsewhere,[47] were dissolved in 0.5 mL of 10 mM potassium phosphate buffer (pH 7) containing 5% $D_2O$ at 4 and 1.4 mM, respectively. Spectra were recorded at 300 K on Bruker DMX-600 and DRX-800 spectrometers equipped with actively shielded 5-mm triple-resonance probes and three-axes pulsed-field gradient (PFG) accessories. The following summarizes the data collection and evaluation protocols used.

The majority of the $^3J$ coupling constants were collected using quantitative *J*-correlation experiments[48] and computer-assisted data evaluation. Solvent suppression was achieved by either gradient coherence selection combined with sensitivity enhancement[49] or WATERGATE.[50] Whenever possible, the water flip-back procedure[51] was included to avoid saturation of fast-exchanging amide hydrogens. Spectrum processing was accomplished using Bruker XWinNMR 1.3 software.

$^3J_{H\alpha,H\beta}$ coupling constants were determined by a 3D HA[HN,HB]-(CACO)NH experiment[52] which correlates the current amino acid's set of $^1H^\alpha$, $^1H^\beta$, and $^1H^N$ chemical shifts in $F_1$ with that of $^{15}$N and $^1H^N$ chemical shifts of the subsequent residue in $F_2$ and $F_3$, respectively. *J* values calculated from the intensity ratio between ($H^\beta$,N,$H^N$) cross-peaks and ($H^\alpha$,N,$H^N$) autocorrelation peaks agreed with data from a related HACAHB experiment[53] run on the same sample, delivering a few additional $^3J_{H\alpha,H\beta}$ coupling constants. Peak heights rather than volumes were inspected throughout.

Pulse sequences employed to measure $^3J_{N',H\beta}$, $^3J_{C',H\beta}$, $^3J_{N',C\gamma}$, $^3J_{C',C\gamma}$, and $^3J_{H\alpha,C\gamma}$ basically derive from existing quantitative *J*-correlation schemes[48] improved to avoid recording additional 2D reference spectra.[54] All experiments share the feature of internal reference peaks accomplished by separate recording of real and imaginary parts in one of the indirectly detected frequency dimensions using two different phase cycles. The fraction of magnetization not transferred via the $^3J$ coupling of interest is void of chemical shift modulation, producing signals at zero frequency in the said indirect dimension, thus constituting an axial peak plane in the 3D heteronuclear *J*-correlation spectrum, in analogy to (2D/3D) homonuclear *J*-correlation, where axial peaks correspond to diagonal peaks. The intensity ratio between related cross and axial peaks, $I_{cross}/I_{axial} = -\tan^2(\pi J\Delta)$, where $\Delta$ is the duration critically tuned for evolution of the respective active coupling, eventually delivering the heteronuclear coupling constants.

$^3J_{N',H\beta}$ coupling constants were obtained from a modified HNHB experiment[55] applied to the $^{15}$N-singly labeled protein sample. The

(46) Konrat, R.; Muhandiram, D. R.; Farrow, N. A.; Kay, L. E. *J. Biomol. NMR* **1997**, *9*, 409−422.

(47) Curley, G. P.; Carr, M. C.; Mayhew, S. G.; Voordouw, G. *Eur. J. Biochem.* **1991**, *202*, 1091−1100.

(48) Bax, A.; Vuister, G. W.; Grzesiek, S.; Delaglio, F.; Wang, A. C.; Tschudin, R.; Zhu, G. *Methods Enzymol.* **1994**, *239*, 79−105.

(49) Kay, L. E.; Keifer, P.; Saarinen, T. *J. Am. Chem. Soc.* **1992**, *114*, 10663−10665.

(50) Piotto, M.; Saudek, V.; Sklenár, V. *J. Biomol. NMR* **1992**, *2*, 661−665.

(51) (a) Grzesiek, S.; Bax, A. *J. Am. Chem. Soc.* **1993**, *115*, 12593−12594. (b) Stonehouse, J.; Shaw, G. L.; Keeler, J.; Laue, E. D. *J. Magn. Reson. A* **1994**, *107*, 178−184.

(52) Löhr, F.; Schmidt, J. M.; Rüterjans, H. *J. Am. Chem. Soc.* **1999**, *121*, 11821−11826.

(53) Grzesiek, S.; Kuboniwa, H.; Hinck, A. P.; Bax, A. *J. Am. Chem. Soc.* **1995**, *117*, 5312−5315.

(54) Löhr, F.; Pérez, C.; Schmidt, J. M.; Rüterjans, H. *Bull. Magn. Reson.* **1999**, 20, 9−14.

critical $J$ evolution delay, set at a half-integer multiple of the large one-bond NH coupling, was $\Delta = 7(2^1J_{NH})^{-1} = 37.5$ ms. $^3J_{C',H\beta}$ coupling constants resulted from a modified HN(CO)HB experiment[56] applied to the $^{13}C,^{15}N$-doubly labeled sample with the critical period for evolution of the long-range heteronuclear couplings set at $\Delta = 22$ ms. Additional $^3J_{C',H\beta}$ coupling constants resulted from an E.COSY-type small-flip-angle 3D ct-HMQC-COSY and 2D line shape fitting in cross sections.[57]

$^3J_{H\alpha,C\gamma}$ coupling constants involving aliphatic $\gamma$ carbons were measured in a HCGHA experiment including the LRCH pulse sequence.[58] Durations for de- and rephasing of $C^\gamma$ magnetization components with respect to long-range coupled protons were 23.6 ms $= 3(^1J_{CH})^{-1}$ and 21.6 ms $= 11(4^1J_{CH})^{-1}$, respectively. $^3J_{H\alpha,C\gamma}$ coupling constants in Asn, Asp, His, Phe, Trp, and Tyr residues resulted from an E.COSY-type 3D ct-HTQC-COSY and 2D line shape fitting in cross sections.[59]

$^3J_{N',C\gamma}$ and $^3J_{C',C\gamma}$ coupling constants were taken from HNCG[46,60] and HNCOCG-type[2,46] spectra, respectively. Separate experiments were carried out for residues with aliphatic (Arg, Gln, Glu, Ile, Leu, Lys, Pro, Thr, Val), aromatic (His, Phe, Trp, Tyr), and carbonyl (Asp, Asn) $\gamma$-carbons. $^3J_{N',C\gamma}$(ali) coupling constants resulted from a sensitivity enhanced $^1H,^{15}N$-TROSY-type[61] HNCG pulse sequence, allowing for comparatively long de- and rephasing delays of 86 ms, while HNCOCG experiments to determine $^3J_{C',C\gamma}$(ali) employed critical delays $\Delta = 37$ ms $= 2(^1J_{C',C\alpha})^{-1}$. To resolve signal overlap in the axial peak plane, two spectra were recorded exploiting either $^{15}N'$ or $^{13}C'$ shifts in the third dimension. $^3J_{N',C\gamma}$(aro) and $^3J_{C',C\gamma}$(aro) coupling constants were collected simultaneously in a novel $^1H,^{15}N$-TROSY-type HN(CO)CG experiment,[62] carried out with $J_{N',C\gamma}$ and $^3J_{C',C\gamma}$ de- and rephasing periods ranging from 58 to 67 ms and from 28 to 32 ms, respectively. $^3J_{N',C\gamma}$ coupling constants in Asp and Asn residues were studied using a modified HNCO-based pulse sequence, in which N,C one-bond correlation is suppressed by matching the $\Delta$ period to $(^1J_{N',C'})^{-1} = 66$ ms.[63] $^3J_{C',C\gamma}$ interactions in Asp and Asn residues were quantified using a HN(CO)CO experiment[6] with $\Delta = 56$ ms.

**Acknowledgment.** Dr. Martin Walsh (EMBL, Hamburg) is thanked for making available the X-ray coordinates resolved at 0.17 nm prior to publication. Dr. Martin Knauf (Frankfurt) and Prof. Stephen Mayhew (University of Dublin) kindly helped in the preparation of the recombinant isotope-enriched flavodoxin. Dr. James Feeney and Dr. Geoff Kelly (NIMR, London) are thanked for critical comments on the manuscript and for stimulating discussions. C.P. acknowledges a grant from the Deutscher Akademischer Austauschdienst (DAAD). This work was supported in part by the Deutsche Forschungsgemeinschaft (Ru 145/11-2) and by funds from the Fonds der Chemischen Industrie to J.M.S.

**Supporting Information Available:** Three tables, showing the weight matrices used to assemble amino-acid-specific Karplus parameters from incremental coefficients, a comparison for the final model $J_4M_1S_1$ of the experimental and back-calculated $^3J$ coupling constants with violations marked, and details on torsion angles $\chi_1$ obtained with the six self-consistent models, in comparison with X-ray data (PDF). This material is available free of charge via the Internet at http://pubs.acs.org.

JA003724J

(55) Archer, S. J.; Ikura, M.; Torchia, D. A.; Bax, A. *J. Magn. Reson.* **1991**, *95*, 636−641.
(56) Grzesiek, S.; Ikura, M.; Clore, G. M.; Gronenborn, A. M.; Bax, A. *J. Magn. Reson.* **1992**, *96*, 215−221.
(57) Schmidt, J. M.; Löhr, F.; Rüterjans, H. *J. Biomol. NMR* **1996**, *7*, 142−152.
(58) Vuister, G. W.; Bax, A. *J. Magn. Reson. B* **1993**, *102*, 228−231.
(59) Löhr, F.; Pérez, C.; Köhler, R.; Rüterjans, H.; Schmidt, J. M. *J. Biomol. NMR*, **2000**, *18*, 13−22.
(60) Hu, J.-S.; Bax, A. *J. Biomol. NMR* **1997**, *9*, 323−328.
(61) (a) Pervushin, K.; Riek, R.; Wider, G.; Wüthrich, K. *Proc. Natl. Acad. Sci. U.S.A.* **1997**, *94*, 12366−12371. (b) Yang, D.; Kay, L. E. *J. Biomol. NMR* **1999**, *13*, 3−10.
(62) Löhr, F.; Rüterjans, H. *J. Magn. Reson.* **2000**, *146*, 126−131.
(63) (a) Cordier, F.; Grzesiek, S. *J. Am. Chem. Soc.* **1999**, *121*, 1601−1602. (b) Cornilescu, G.; Hu, J.-S.; Bax, A. *J. Am. Chem. Soc.* **1999**, *121*, 2949−2950.